ARL-SR-0454 ● JAN 2022

5th Annual Postdoc and Early Career Research Day: CCDC Army Research Laboratory's Poster Symposium and Activities

by Daniel Ames, Ahmed Anwar, Anthony Baker, Anjon Basak, Chloe Callahan-Flintoft, Anthony Clay, Stephen Cluff, Benjamin Evangelisti, Mary Beth Galanko, Felix Gervitz, Philip Guerieri, Zach Hare, Cory Hayes, Robin Karhu, Cory Knick, LeighAnn Larkin, David McLeod, Quang Nguyen, Vijay Parameshwaran, Katie Price, TJ Rohrabaugh, Jonah Sengupta, Piyush Sharma, Richard Thomas, Owen Vail, Dashiell Vitullo, Adam Wilson, Alexander Winton, and Michael Yeager

Approved for public release: distribution unlimited.

NOTICES

Disclaimers

The findings in this report are not to be construed as an official Department of the Army position unless so designated by other authorized documents.

Citation of manufacturer's or trade names does not constitute an official endorsement or approval of the use thereof.

Destroy this report when it is no longer needed. Do not return it to the originator.

ARL-SR-0454 ● JAN 2022

Daniel Ames, Mary Beth Galanko, Philip Guerieri, Robin Karhu, Cory Knick, LeighAnn Larkin, Quang Nguyen, Vijay Parameshwaran, Katie Price, TJ Rohrabaugh, Richard Thomas, Owen Vail, Adam Wilson, and Alexander Winton
Sensors and Electron Devices Directorate, DEVCOM Army Research Laboratory

Anthony Clay, Stephen Cluff, Benjamin Evangelisti, David McLeod, Jonah Sengupta, and Michael Yeager
Weapons and Materials Research Directorate,
DEVCOM Army Research Laboratory

Anthony Baker and Chloe Callahan-Flintoft
Human Research and Engineering Directorate,
DEVCOM Army Research Laboratory

Ahmed Anwar, Anjon Basak, Felix Gervits, Zach Hare, Cory Hayes, Piyush Sharma, and Dashiell Vitullo
Computational and Information Sciences Directorate,
DEVCOM Army Research Laboratory

Approved for public release: distribution unlimited.

REPORT DOCUMENTATION PAGE

Form Approved
OMB No. 0704-0188

Public reporting burden for this collection of information is estimated to average 1 hour per response, including the time for reviewing instructions, searching existing data sources, gathering and maintaining the data needed, and completing and reviewing the collection information. Send comments regarding this burden estimate or any other aspect of this collection of information, including suggestions for reducing the burden, to Department of Defense, Washington Headquarters Services, Directorate for Information Operations and Reports (0704-0188), 1215 Jefferson Davis Highway, Suite 1204, Arlington, VA 22202-4302. Respondents should be aware that notwithstanding any other provision of law, no person shall be subject to any penalty for failing to comply with a collection of information if it does not display a currently valid OMB control number.
PLEASE DO NOT RETURN YOUR FORM TO THE ABOVE ADDRESS.

1. REPORT DATE *(DD-MM-YYYY)*	2. REPORT TYPE	3. DATES COVERED (From - To)
January 2022	Special Report	16 September 2020

4. TITLE AND SUBTITLE
5th Annual Postdoc and Early Career Research Day: CCDC Army Research Laboratory's Poster Symposium and Activities

5a. CONTRACT NUMBER

5b. GRANT NUMBER

5c. PROGRAM ELEMENT NUMBER

6. AUTHOR(S)
Daniel Ames, Ahmed Anwar, Anthony Baker, Anjon Basak, Chloe Callahan-Flintoft, Anthony Clay, Stephen Cluff, Benjamin Evangelisti, Mary Beth Galanko, Felix Gervitz, Philip Guerieri, Zach Hare, Cory Hayes, Robin Karhu, Cory Knick, LeighAnn Larkin, David McLeod, Quang Nguyen, Vijay Parameshwaran, Katie Price, TJ Rohrabaugh, Jonah Sengupta, Piyush Sharma, Richard Thomas, Owen Vail, Dashiell Vitullo, Adam Wilson, Alexander Winton, and Michael Yeager

5d. PROJECT NUMBER

5e. TASK NUMBER

5f. WORK UNIT NUMBER

7. PERFORMING ORGANIZATION NAME(S) AND ADDRESS(ES)
DEVCOM Army Research Laboratory
ATTN: FCDD-RLS-ED
Adelphi, MD 20783-1138

8. PERFORMING ORGANIZATION REPORT NUMBER
ARL-SR-0454

9. SPONSORING/MONITORING AGENCY NAME(S) AND ADDRESS(ES)

10. SPONSOR/MONITOR'S ACRONYM(S)

11. SPONSOR/MONITOR'S REPORT NUMBER(S)

12. DISTRIBUTION/AVAILABILITY STATEMENT
Approved for public release: distribution unlimited.

13. SUPPLEMENTARY NOTES
ORCIDs: Chloe Callahan-Flintoft, 0000-0002-1874-2032; Anthony Clay, 0000-0003-2340-7009; Stephen Cluff, 0000-0001-8666-8244; Mary Galanko, 0000-0002-7769-3963; Philip Guerieri, 0000-0001-6145-993X; James Hare, 0000-0002-3920-7442; David McLeod, 0000-0001-5293-6060; Katherine Price, 0000-0001-6140-0020; Thomas Rohrabaugh, 0000-0001-6652-9781; Dashiell Vitullo, 0000-0001-8797-9968; Adam Wilson, 0000-0003-4741-6612

14. ABSTRACT
The US Army Combat Capabilities Development Command (CCDC) Army Research Laboratory (ARL) Postdoc Association (PDA) organized its 5th Annual Postdoc and Early Career Research Day on 16 September 2020 to showcase research outcomes, achievements, and contributions from postdocs and early career researchers across the enterprise. The event included a series of invited speakers, a Q&A panel, and a poster session. This special report contains a brief summary outlining the event and a snapshot of the CCDC Army Research Laboratory's postdoctoral and early career research communities in the fall of 2020. The abstracts presented at the event and a limited number of contributed posters are appended.

15. SUBJECT TERMS
ARL Postdoc and Early Career Research Day, ARL Postdoc Association, ARL Early Career Working Group, 2020 Postdoc Week, poster symposia

16. SECURITY CLASSIFICATION OF:			17. LIMITATION OF ABSTRACT	18. NUMBER OF PAGES	19a. NAME OF RESPONSIBLE PERSON
a. REPORT	b. ABSTRACT	c. THIS PAGE			LeighAnn Larkin
Unclassified	Unclassified	Unclassified	UU	62	19b. TELEPHONE NUMBER (Include area code) (301) 394-1430

Standard Form 298 (Rev. 8/98)
Prescribed by ANSI Std. Z39.18

Contents

List of Figures iv

List of Tables iv

Acknowledgments v

1. Introduction 1

2. Engagement across the Laboratory 2

3. Hosting the Research Symposium Virtually 4

Appendix A. Contributed Abstracts Presented at the 5th Postdoc and Early Career Research Day 5

Appendix B. Contributed Posters Presented at the 5th Postdoc and Early Career Research Day 25

List of Symbols, Abbreviations, and Acronyms 54

Distribution List 55

List of Figures

Fig. 1 Number of abstracts submitted to the postdoc research symposium over the past 3 years (representation from the various directorates is shown) 4

List of Tables

Table 1 List of postdoctoral fellows who presented at the symposium 3

Acknowledgments

The 5th Annual Postdoc and Early Career Research Day Organizing Committee would like to acknowledge those who assisted with planning, coordinating, and volunteering at the symposium. The committee would like to thank the US Army Research Laboratory's director, Dr Patrick Baker, for speaking at the event as an invited speaker. The committee would like to thank panelists Dr Barbara Nichols, Dr Mark Tschopp, Ms Heidi Maupin, and Dr Dave Hairston for a great Q&A session. We would like to thank the work of the administrative staff in the Outreach Office, notably Dr Patrice Collins and Mr Joseph Gamson, for organizing "ARL Jeopardy" during the luncheon. The committee would like to acknowledge our judges, Dr Rich Becker, Dr Stephen Berkebile, Dr Piotr Franaszczuk, Dr Asher Leff, Dr Qudsia Quaraishi, Dr Jeffrey Veals, Dr Chi-Chin Wu, and Dr Rose Pesce-Rodriguez, who volunteered their time. The committee would also like to acknowledge Dr Pesce-Rodriguez for her advice, guidance, and support. Lastly, we would like to acknowledge Dr Greg Liebermann and Ms Ashley Eidsmore for assisting in setting up the ARL Cafe environment.

1. Introduction

The 5th Annual Postdoc and Early Career Research Day (5PECRD) was a US Army Combat Capabilities Development Command (CCDC) Army Research Laboratory (ARL) Postdoc Association (PDA) initiative to commemorate postdoctoral- and early-career-executed and -led research across CCDC ARL. The PDA is an organization that was established by and is composed of ARL postdocs and aims to elevate the experience of postdocs and early career researchers at ARL. The annual research day is the PDA's annual flagship event to celebrate the research performed by our postdocs.

The 5PECRD was held on September 16, 2020, and coincided with the 2020 National Postdoc Appreciation Week (NPAW) in celebration of CCDC ARL's postdoctoral cohort. Similar to NPAW, the goal of 5PECRD was to bring awareness to the important research being performed by postdocs and early career researchers across the organization, promote collaboration where suited, and create a space for postdocs to network within ARL. Mainly, the 5PECRD was a venue to celebrate and promote the postdoctoral and early career experience at ARL.

This was the fifth iteration of this event and was held virtually on ARL Cafe. Owing to the virtual nature of the event, each presenter submitted a soundbite with an "elevator pitch" of their research in addition to the poster. The 5PECRD included a panel session where postdoctoral fellows interacted with CCDC ARL civilians with a diverse perspective of what enables success at the laboratory. Each of the panelists represented a different stage and trajectory of career and brought a unique and rich perspective to the discussion. The Outreach Office organized a social lunch with an ARL-inspired game of "Jeopardy". This event was well received and provided newcomers with additional background information on the history and organization of the laboratory.

A total of 30 postdocs presented posters, and many others attended other activities such as the Q&A panel and the invited keynote event.

The 5PECRD objectives were as follows:

- Recognize contributions from postdocs and early career researchers to current state-of-the- art research and discovery at CCDC ARL.
- Foster collaborative research among postdocs with common research interests.
- Serve as an interactive platform for postdocs and upper management.

- Provide insights into how to develop a successful career as an Army scientist.
- Encourage a sense of belonging among early career researchers and postdocs within the research community at CCDC ARL.

This Special Report provides a snapshot of the 5PECRD. An abstract book and limited number of contributed posters are published in Appendixes A and B.

2. Engagement across the Laboratory

A total of 30 postdocs and early career researchers presented posters and "elevator pitches". Those who agreed to be included in this technical report are listed in Table 1 with their location and directorate affiliation. Although there was a reduction in the number of postdoctoral fellows across the lab, there was a slight increase in the number of abstracts submitted from 2019 (29 vs. 30) and 2017 (26 vs. 30). The distribution across the directorates at Aberdeen Proving Ground (APG) and Adelphi Laboratory Center (ALC), Maryland, included 14 abstracts from the Sensors and Electron Devices Directorate (SEDD), 7 from the Weapons and Materials Research Directorate (WMRD), 7 from the Computational and Information Sciences Directorate (CISD), and 2 from the Human Research and Engineering Directorate (HRED). Trends observed in number of abstracts submitted per directorate can be observed in Fig. 1. A limited number of the abstracts and posters can be found in Appendixes A and B, respectively.

Table 1 List of postdoctoral fellows who presented at the symposium

Presenter	Directorate	Location
Ames, Daniel	SEDD	ALC
Anwar, Ahmed	CISD	ALC/APG
Baker, Anthony	HRED	APG
Basak, Anjon	CISD	ALC/APG
Callahan-Flintoft, Chloe	HRED	APG
Clay, Anthony	WMRD	APG
Cluff, Stephen	WMRD	APG
Evangelisti, Benjamin	WMRD	APG
Galanko, Mary Beth	SEDD	ALC
Gervits, Felix	CISD	ALC/APG
Guerieri, Philip	SEDD	ALC
Hare, Zach	CISD	ALC
Hayes, Cory	CISD	ALC/APG
Karhu, Robin	SEDD	ALC
Knick, Cory	SEDD	ALC
Larkin, LeighAnn	SEDD	ALC
McLeod, David	WMRD	APG
Nguyen, Quang	SEDD	ALC
Parameshwaran, Vijay	SEDD	ALC
Price, Kate	SEDD	ALC
Rohrabaugh, TJ	SEDD	ALC
Sengupta, Jonah	WMRD	APG
Sharma, Piyush	CISD	ALC
Thomas, Richard	SEDD	ALC
Vail, Owen	SEDD	ALC
Vitullo, Dashiell	CISD	ALC
Wilson, Adam	SEDD	ALC
Winton, Alexander	SEDD	ALC
Yeager, Michael	WMRD	APG

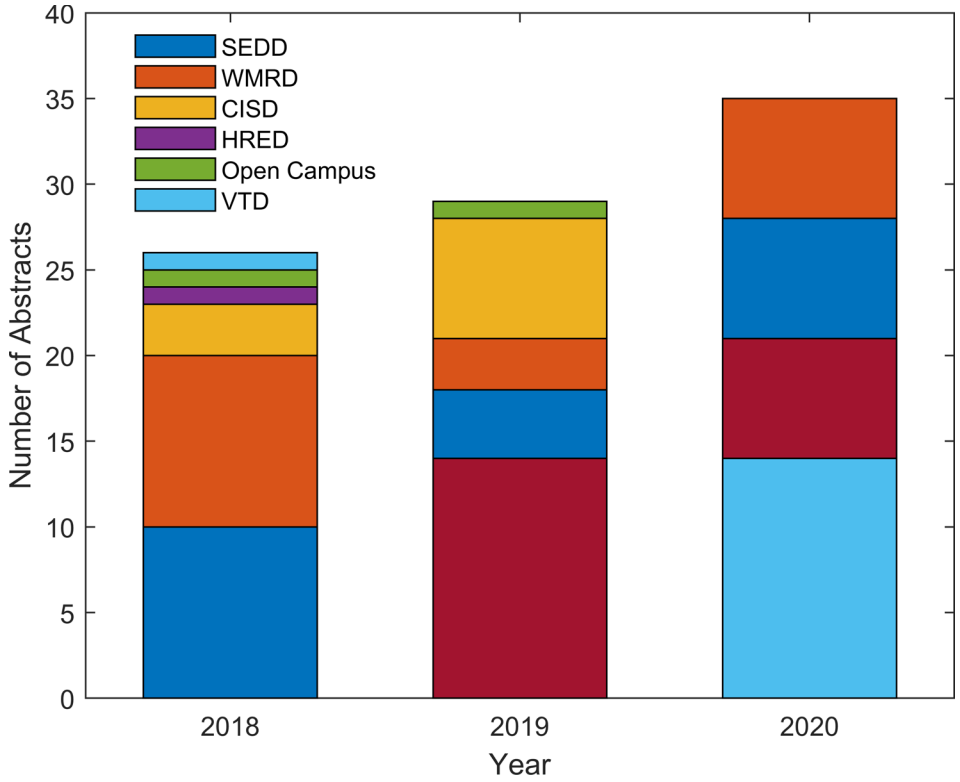

Fig. 1 Number of abstracts submitted to the postdoc research symposium over the past 3 years (representation from the various directorates is shown)

3. Hosting the Research Symposium Virtually

Traditionally, this event is held onsite at either ALC or APG. The location is alternated each year to maximize accessibility. Owing to the COVID-19 pandemic, the symposium was held, for the first time, virtually. The poster session, panel, and invited keynote speaker were all hosted over a channel within ARL Cafe. The posters and elevator pitches were available on the channel for general viewing throughout the day.

Virtual conferences have a disadvantage in that they offer no face-to-face networking, but there is increased accessibility for attendees and presenters. Additionally, it offers the broader ARL community, not present at the chosen location, to attend a select number of events for the day. This was advantageous for our invited keynote from Dr Patrick Baker, which a large audience at ARL attended.

Additionally, presenters were asked to submit a 2-min “elevator pitch” along with their poster. This aspect was introduced after a series of discussions at PDA Town Halls where early career researchers and postdocs expressed interest in more opportunities to practice quickly summarizing their research to different communities.

Appendix A. Contributed Abstracts Presented at the 5th Postdoc and Early Career Research Day

The contents of this appendix appear in original form, without editorial change.

Laser forming of compliant mechanisms

Daniel Calvin Ames[1], *Gabe Smith*[1], *Nathan Lazarus*[2]
[1] FCDD-RLS-EM, [2] FCDD-RLS-CC

Compliant mechanisms, inspired by the ancient art of origami are useful structures designed to replace traditional mechanical components. Such flexible mechanisms are created with 3D printing, milling, stamping, injection molding, and other ways. However, very thin complex mechanisms have been difficult to create in metal. The work of this research performed at ARL is to explore and quantify the use of lasers to cut and form metal compliant mechanisms. Lasers have been used to cut and bend metal, but up to this point just rigid structures have been created with laser forming. The presented work demonstrates five relatively simple compliant mechanisms adapted to be cut and formed by an Nd:YAG laser. Thin stainless steel sheet metal is used initially as the design medium. Models are also presented showing the anticipated displacement behavior for the stainless steel mechanisms when a force or moment is applied. The benefits and challenges of this technology are explored. Potential applications are also discussed.

Software diversity for network security: A game theoretic framework

Ahmed H. Anwar, *Nandi Leslie*, *Charles Kamhoua*, FCC-RLC-ND

Diversity-based defenses are essential to network security, a negligible mechanism a few decades ago that has recently emerged as an intuitive approach that presents necessary concepts for resilience; these types of defenses introduce uncertainty and probabilistic protection from the attacker and provide a rich framework for diversifying program transformations. In this project, we investigate the advantage of software diversity in network security. Diversity increases the operational and configurational cost of the network, and hence, the network administrator encounters a trade off between network security and the cost needed to have a well-diversified network. Such a trade off is studied in a two-player nonzero-sum game-theoretic framework. In this game, the opponent (i.e., adversary) spends more effort to compromise a diversified network, and the game model studies the effect of diversity on network security under attack. An algorithm is presented to solve the game model and obtain the Nash equilibrium diversity strategy. The existence of Nash equilibrium as a security strategy for the defender is analyzed, and a software diversity algorithm is developed via embedding graph-coloring approach based on Nash equilibrium strategy for diversity. The complexity of the proposed algorithm is analyzed, and a complexity reduction approach is developed, which has shown to yield an almost exact reward for the defender, as verified via numerical results. Finally, numerical results are presented that validate the effectiveness of the proposed software diversity approach.

A toolkit for assessing communication in human-Autonomy teams

Anthony L. Baker[1], *Daniel E. Foster*[2], *Catherine E. Neubauer*[2], *Sean M. Fizhugh*[3], *Andrea Krausman*[3], *Kristin E. Schaefer*[3]

[1] FCDD-RLH-FD, [2] FCDD-RLH-FA, [3]FCDD-RLH-FD

Communication is the means through which team members build larger team dynamics that facilitate cohesion and trust while performing joint tasks. Thus, how we evaluate team communication can provide critical insights into effective performance. Although many communication-based measures have been tested and validated for human teams, this poster identifies key approaches for human-autonomy teams, specifically those applicable to multi-size teams across a variety of military operations. This toolkit comprises four approaches for deriving critical information about how team interactions affect, and are affected by, cohesion, trust, and performance: 1) Aggregate communication flow, which can be quickly assessed to identify the proportion of a team's communication accounted for by each possible combination of team members; 2) Relational event modeling, which allows for analysis of dynamic networks and reveals time-ordered trends and relationships that are not observable using aggregated approaches; 3) Linguistic similarity, which tracks synchrony between humans and autonomy, using information derived from communication content to inform how autonomy should adapt their communication styles; 4) Analysis of human team members' voices or facial expressions, which we are developing to provide critical real-time detection of emotional states relevant to teamwork. These tools can be used to understand when trust and/or cohesion break down during a mission and when interventions are necessary to appropriately calibrate trust and cohesion, supporting the goals of the Human-Autonomy Teaming Essential Research Program and the Next Generation Combat Vehicle modernization priority.

Deceptive maneuver in Multi-Domain Operations (MDO) using Multi-Agency Reinforcement Learning (MARL) to gather superiority over the adversary

Anjon Basak, *Derrik Asher*, CISD-ISD-CUB

Adversaries pose a security threat to national interests and resources. As a part of the defense strategy, the defender needs to use maneuvers to gain superiority in the Multi-domain Operations (MDO). However, adversaries are becoming smarter and resilient because of scientific and technological advancements. Superior resources alone are not enough to defeat them in MDO. The defense force needs to use autonomous strategic maneuvers using deception to gain superiority over the enemy as a part of the US Army's modernization efforts in MDO. AI for Autonomous Maneuver and Mobility (AIMM) is an Essential Research Program (ERP) that focuses on enabling the Next Generation Combat Vehicles (NGCVs)

with autonomous mobility and maneuvering capabilities. These future autonomous systems will have to predict and plan in collaboration with human agents and provide support to them by autonomously maneuvering in MDO. Our objective is to use collaborative strategic maneuvers that utilize deception in reconnaissance and combat activities in MDO to gain advantages over the adversary. In this paper, we present a road map to address the alignments of objectives between AIMM and Multi-agent Reinforcement Learning (MARL) for autonomous maneuvering. Then we present a classification of MARL algorithms and their trade-offs in MDO to give a deeper insight into the most promising MARL algorithms. Then we present a methodological road map with a timeline on how the most promising MARL algorithms can be further improved (e.g. incorporating deception) to address the algorithmic shortcomings in the way of gaining superiority over the enemy.

RAGNAROC: A computational to understand how attentional mechanisms will respond to augmented reality displays

Chloe Callahan-Flintoft[1], *Michael Guess*[2], *Gabriella B. Larkin*[3]
[1] FCCD-RLH-FC, [3] FCDD-RLD-D

A soldier's field of view offers a complex and dynamic array of visual information. Reflexive spatial attention is thought to be the collection of mechanisms by which the brain prioritizes some information over others for enhanced processing. This form of attention has been shown to be guided by both the bottom-up saliency of a stimulus (Theeuwes, 1994) and one's top-down goals (Folk, Remington, & Johnston, 1993). The Reflexive Attention Gradient through Neural AttRactOr Competition (RAGNAROC), is a framework by which to understand how the brain mediates between these two factors. The model uses hierarchical neural circuits specifically adapted for rapid, parallel decision making to simulate how locations of the visual field compete for attention. The result of this competition is an excitatory attractor state established at attended locations and suppression applied to others. The current work demonstrates how the model is able to account for seemingly conflicting results in the literature (i.e. how some experimental paradigms show evidence of attentional capture while others show evidence of suppression to salient distractors) by simulating both behavioral and electrophysiological patterns found in experimental data. With the introduction of augmented reality, it is now possible for artificial intelligence systems to direct a Soldier's visual attention to task relevant locations or potential threats. RAGNAROC demonstrates how certain displays may in fact encourage the suppression of information rather than its enhancement by generating explicit predictions of users' eye movement patterns when information is overlaid on a dynamic scene.

Development of Michael addition binder system for additive manufacturing of energetic materials

Anthony M. Clay[1], *Joshua R. Mitchell*[1], *David M. VanOosten*[1], *Ian M. McAninch*[1], *John J. La Scala*[1], *E. Jason Robinette*[2]

[1] FCDD-RLW-MD, [2] FCDD-RLW-D

Theoretical predictions show that 3D printed geometries can result in improved performance, increasing muzzle velocity and range of munitions. As a result, we are developing 3D printing resins with high loadings of energetic solid particles where the resin cures quickly after being deposited by the printer. However, binders for energetic composites necessitate material properties not commonly encountered in commercially available materials, such as glass transition temperatures below -40 ^{o}C and elongation upwards of 100%. While photochemical techniques feature amongst the fastest cure kinetics, high solids loading and high viscosities are problematic for such manufacturing methods. Ambient reactive extrusion (ARE) has displayed the ability to extrude highly viscous material which allowed the 3D printing of polymers based on isocyanate chemistry. 3D printing of acrylates would reduce toxicity and mitigate safety concerns associated with isocyanates. 3D printing solely based on acrylate Michael addition chemistry has yet to be realized. In this study amine acrylate binder systems are developed for 3D printing of energetic materials. Synthesis of novel binders primed for superior reactivity allowed for the tailoring of both reaction kinetics and material properties. Investigations unveiled an inversely proportional relationship between gel time, which correlates with rate of polymerization, and molecular weight between crosslinks. Printable resin mixtures were formulated and successfully printed into representative rocket propellant cylinder geometries with a center perforation of 12 mm and a height of 30 mm. Initial knowledge gained from the inert binder system spurred the development of energetic binders of similar chemistry that have the potential to further increase the velocity and range of munitions.

Reconstruction of prior Austenite in high-strength AF96 steel

Stephen Cluff [1], *Andelle Kudzal*[2], *Daniel Field*[2], *Vikas Sinha*[3]

[1] FCDD-RLW-MD, [2] FCDD-RLW-MF, [3] Air Force Laboratory, Materials and Manufacturing Directorate, ARFL/RXCM, Wright-Patterson Air Force Base

Awarded Best Poster.

The prior Austenite microstructure of room-temperature steel can be obtained computationally from EBSD data. This “reconstruction” of the prior-phase microstructure depends on a crystallographic orientation relationship between the parent and daughter phases. The ability to perform this reconstruction allows for the observation of aspects of austenite texture that are difficult to observe directly.

Such reconstruction techniques thus provide additional ways to quantify the effect of processing schemes on the final room temperature of steel. A novel high-strength steel designated as AF9628 is the subject of present reconstructions. The current work presents and compares the reconstructions of both wrought and additively manufactured AF9628. The usefulness of prior austenite reconstruction to survey the microstructure of additively manufactured AF9628 is discussed.

The effects of surface functionalization on the diffusion of Oxygen into the Aluminum oxide shell of Aluminum nanoparticles

Benjamin Evangelisti[1], *Chi-Chin Wu*[2]

[1]Dept. of Chemistry, The Pennsylvania State University, [2] FCDD-RLW-WA

Awarded best elevator pitch.

This work explores the effects of different small molecules on the oxidation of aluminum nanoparticles (nAl) via reactive molecular dynamics (MD) simulations. This comparative study of nAl surface functionality and its roles in oxygen diffusion is important because carbon-functionalized nAl shows increased reactivity in experiments despite a passivating amorphous aluminum oxide (Al_2O_3) shell forming at its surface. An ARL built-in-house, Python-based software package, the Composite Model Builder and Analysis Toolkit (COMBAT), was utilized in conjunction with the Large-scale Atomic/Molecular Massively Parallel Simulator (LAMMPS) to generate models and perform MD simulations of reactions between select small molecules and the nAl surface using the reactive force field (ReaxFF). Multiple model samples with different aluminum oxide layer thicknesses were created with different experimentally-determined carbon-containing small molecules adsorbed to the oxide surface in an oxygen-rich environment utilizing the Al/O ReaxFF potential. Preliminary results show the resulting carbon surface-coating is highly localized to within 0.5 nm of the surface and reduces diffusion rates of oxygen into the aluminum oxide layer. When this surface coating is prepared using water instead of a carbon-containing species, the surface-coating is localized directly at the surface and further reduces the ability of oxygen to diffuse into the oxide layer. This work validates hypothetical mechanisms derived from existing experimental evidences and provides insights for the effects of surface modification and coating on oxidation diffusion into the oxide layer of nAl.

Quartz piezoelectric resonators for RF front-end applications up to 200 MHz

Mary Beth Galanko[1], *Sarah S. Bedair*[1], *Daniel A. Diamond*[1], *Ryan Rudy*[2], *Victor Farm-Guoo Tseng*[1], *Jeffrey S. Pulskamp*[2], *Iain Kierzewski*[1]

[1]FCDD-RLS-CC, [2] FCDD-RLS-EM

This work investigates the performance of AT-cut quartz resonators as one-port and two-port voltage gain devices for wake-up receiver applications. Wake-up receivers enable persistent, distributed communication at "near-zero" power (< 100 nW), serving a variety of applications from consumer "Internet of Things" (IoT) to Army environment monitoring. Unattended ground sensors can greatly benefit from wake-up radios because they enable reduced power consumption and limit the frequency of battery replacement. Given demands of high sensitivity, minimizing power consumption and false-alarm rate remains a challenge in WUR design. The piezoelectric devices in this work offer passive voltage gain, impedance matching, and high-Q resonant filtering in the wake-up radio front-end. These quartz resonators are fabricated in a mature, commercially available process, promoting widespread integration into radio-frequency (RF) wake-up receivers (WURs). At 50 MHz, various 1-port resonators demonstrate voltage gains >100x (referenced to 50 Ω) in direct measurements using a high-impedance active probe. These devices have quality factor (Q) up to 140,000 and electromechanical coupling $\left(k_{eff}^2\right)$ up to 0.445%. A similar 1-port quartz resonator design at fs~ 75 MHz shows gain over 300 V/V (referenced to 50 Ω) and Q around 335,000 at a ~60 fF load. This device has the highest voltage gain directly measured to date in a piezoelectric micromechanical resonator. Furthermore, recent measurements show that high gain and Q are possible at up to 200 MHz, making this technology a promising option for WuRs over a wide frequency range.

Exploring how robots should ask questions to maximize learning

Felix Gervits, FCDD-RLC-IT

Robots working alongside humans in novel environments will readily come across objects, actions, and tasks that they do not know about. As a result, mechanisms are needed for the robots to learn about these novel concepts through dialogue with humans. In order to inform the development of algorithms to address this problem, we are conducting a human-subjects study to understand how robots (controlled by humans) ask questions to maximize learning. Due to current restrictions on in-person experiments, the study will be conducted online through Amazon Mechanical Turk. However, to maintain an interactive element in the study, we have developed a software framework which allows online participants to communicate with an experimenter in real time in an immersive 3D environment.

Participants will perform a collaborative task in which they play the role of a robot on board a simulated spacecraft, while communicating with a Commander (an experimenter). The Commander will instruct the participants using novel concepts (e.g., "Place the modular spanner in locker A"), and we are interested in exploring the kinds of questions people (playing the role of a robot) will ask to clarify these instructions. The study is exploratory, and we hope to elicit a variety of question types including questions about object properties (e.g., size, color, etc.), spatial orientation, procedural knowledge, and others. Our working hypothesis is that human-generated questions from this study design can be used by robots to effectively learn new concepts.

Detonation of porous Silicon nanoenergetics

Philip M. Guerieri[1], *Wayne A. Churaman*[1], *Brian Fuchs*[2]
[1] FCDD-RLS-EM, [2]FCDD-ACD-IM

Use of nanothermite metal-based energetics for increased energy density in explosives has been limited by their failure to react on detonation-relevant time scales and hazards associated with nanoparticle powders. Porous silicon (PS) can be fabricated in safer micro- and macroscale formats with specific surface areas exceeding many common energetic metal nanopowders and can be integrated directly on-chip for safe manufacture alongside electronics and MEMS for next-generation initiators in modernized munitions. PS infilled with sodium perchlorate oxidizer is also theorized to be a detonable explosive, which has garnered interest based on its particularly high theoretical detonation energy. The existence of detonation in energetic porous silicon remains contested and would be the first known case of detonation in an exclusively metal fueled formulation. This work presents calculations conducted using Cheetah thermochemical code which predict unique detonation performance characteristics of PS/sodium perchlorate composites (1.7-2.5 km/s detonation velocity; 0.73-1.4 GPa C-J pressure; 0.8-2.0 mass-based TNT equivalent detonation energy), including the existence at some porosity levels of a sonic pre-compression wave ahead of the detonation, highly atypical of detonating materials. Preliminary experimental observation of this pre-compression wave by schlieren high-speed imaging is also presented. Published experimental propagation speeds agree well with maximum detonation performance computed by Cheetah, thereby supporting that energetic PS can and may already be detonating in experiments. While low relative to conventional explosives, the detonation pressures predicted are over 50 times greater than pressures estimated in reactions of fast-burning nanothermites. The high detonation speed predictions for PS (>1.5 km/s) also persist at densities up to 1.4 g/cc, whereas nanothermite burn rates drastically fall off with densification. Among metal-based

composite energetics, explosive porous silicon therefore exhibits the most promise for replacing primary explosives at reasonable densities in igniters and initiators on the basis of reaction rate and detonation pressure.

Communication constrained learning for distributed hypothesis: Testing with uncertain models

James Zachary Hare, *Lance Kaplan*, FCDD-RLC-CA

This work considers the problem of distributed classification with a group of heterogeneous agents connected over a social network. This problem is abstracted to a distributed hypothesis testing problem, where the agents collaborate sequentially to collectively agree on the hypothesis that best matches the model of the ground truth target class. Each agent constructs, shares, fuses, and up-dates a belief for each hypothesis in a non-Bayesian framework. However, we consider that the underlying model of each hypothesis is uncertain, due to the agents' having limited access to training samples. Furthermore, we consider that the network of agents are deployed into a band limited environment, requiring limited communication that creates a highly dynamic network. To accommodate for these challenges, we first present the concept of uncertain models, which incorporates the agent's epistemic uncertainty in the probability distribution of each hypothesis. Then, we propose an event-triggered communication protocol that only transmits a belief for a hypothesis if new information has been incorporated since the previous communication time. We then adapt the agents' belief update rule to accommodate for limited communications. We experimentally validate that the proposed solution allows the agents beliefs to converge within a neighborhood of a network with full communication, while significantly reducing the amount of transmissions. This work impacts the Army since it may be applied to expeditionary missions in the future, where a network of soldiers and/or agents collaborate together for situational awareness in highly dynamic environments.

Preference learning for autonomous ground robot navigation tasks

Cory Hayes, FCDD-RLC-IT

A critical component of teamwork is the ability of group members to understand and predict the intention behind the actions of other members to ensure that the team works as one cohesive unit while addressing multiple subtasks simultaneously. For robots to effectively team with humans, they will need to be considered trustworthy, and two critical elements of robot trustworthiness are reliability and predictability. An autonomous robot that performs the same actions repeatedly may be predictable but not necessarily reliable, especially if it executes

those actions in a vacuum completely unaware of team behavior or environment dynamics. However, an intelligent robot teammate that can learn to adapt to the needs of the team and changes in the environment could prove to be a valuable asset that minimizes user burden.

The overall goal of this work is to first focus on adaptation based on teammate needs by adding a motion planning component for autonomous robot navigation that takes into account the user's preferences for how navigation should be carried out, and evaluate its effectiveness in an environment exploration task where the user gives verbal instructions. We seek to combine human-robot interaction and preference-based reinforcement learning so that an autonomous robot can learn to adapt its behavior based on how the user has reacted to the robot executing previous instructions and the processing of simple environment features.

Annealing behavior of point defects and defect complexes in electron irradiated 4H-SiC

Robin Karhu[1], *Daniel Habersat*[2], *Donald Fahey*[1], *Albert Burk*[1], *Brenda VanMil*[1]
[1] FCDD-RLS-SQ, [2] FCDD-RLS-ED

Point defects in wide bandgap semiconductors have in recent years attracted interest for their spin coherence properties (1). The most well studied example is substitutional Nitrogen with a nearest neighbor vacancy (NV) complex in diamond. Similar properties can be found in point defects in other wide bandgap semiconductors such as Silicon Carbide (SiC). Benefits of using Silicon Carbide as opposed to diamond is the much more mature manufacturing process, such as commercially available substrates and homoepitaxial layers up to 150 mm in diameter and electronic devices such as MOSFETs. Using the point defects is SiC has the benefit of merging existing processing capabilities with emerging quantum information technology.

The defects of interest in SiC are the Silicon vacancy (VSi) and the divacancy (VSiVC) (1-3). These defects are created by irradiating SiC samples with electrons followed by annealing at different temperatures. At the moment there is a lack of understanding in the creation process of these defects. In this work the defect evolution in SiC homoepitaxial layers irradiated with electrons are tracked using Deep level transient spectroscopy (DLTS) and photoluminescence (PL). The study will compare DLTS and PL spectra as a function of temperature and electron irradiation dosage.

(1) Weber, J.R., et al., Quantum computing with defects, *Proc. Natl. Acad. Sci. USA*, 2010. 107(19): p. 8513-8.
(2) Son, N.T., et al., Divacancy in 4H-SiC, *Phys Rev Lett*, 2006. 96(5): p. 055501.
(3) Janzén, E., et al., The silicon vacancy in SiC, *Physica B: Condensed Matter*, 2009. 404(22): p. 4354-4358.

Stimuli-Responsive phase-change materials for adaptive imaging systems

Cory R. Knick[1], *Adam A. Wilson*[2], *Gabriel L. Smith*[3], *Daniel Jean*[3]
[1]RDRL-SER-L, [2] FCDD-RLS-CP,[3] FCDD-RLS-EM

Stimuli-responsive phase change materials are classified by their ability to adapt or reconfigure in response to external stimuli (temperature, light, pH, magnetic/electric fields, etc.) and will enable the next generation of adaptive imaging systems. Phase-change materials can serve as the foundational building block of microactuators which can be used to dynamically reconfigure optical elements to enable reconfigurable imagers with multi-functionality. Application spaces for these materials encompasses variable light transmission, MEMS micromirrors, laser beam steering, adaptive optics, spatial light modulators (SLM), micro-robotics, and actuation. Current efforts explore vanadium dioxide (VO_2), and metallic shape memory alloys (SMA), but future emphasis on other novel material classes or metamaterials is also of interest to enable fast, tunable light filters. Research in the Imaging Technologies Branch at NVESD focuses on novel device architectures to enable proof on concept demonstrations and fundamental materials research and nanofabrication techniques to tailor specific material properties. Thermal property measurements (like those based on TDTR and FDTR) on the nanoscale will help enable improved device modeling, simulation, design, and performance. Transition pathways for these research efforts include Next Generation Combat Vehicle (NGCV) and Integrated Visual Augmentation Systems (IVAS).

Compositionally-mixed interfaces and thermal boundary conductance at Pt-silicide/Si Interfaces

LeighAnn Larkin[1], *Pamela Norris*[2]
[1] FCDD-RLS-ED, [2] Dept. of Mechanical and Aerospace Engineering, University of Virginia

As devices continue to shrink in size towards the nano-length scale, solid-solid interfaces serve as a primary scattering center for energy carriers (phonons), often creating a thermal bottleneck within the device. The optimization of thermal boundary conductance, h_{BD}, at solid-solid interfaces is complicated by the innate

phonon spectra of materials, which limits the theoretical maximum h_{BD} achievable for a solid-solid interface. To offset this constraint, researchers have shown that inserting a thin interstitial layer with intermediate vibrational properties can serve as a "phonon bridge" and enhance h_{BD}(1). Compositionally-graded interfaces present the opportunity to transition the phonon density of states and have been predicted to potentially enhance h_{BD} by 300% at vibrationally mismatched interfaces(2).

A series of Pt-based metallic silicides/Si interfaces were annealed to encourage diffusion and the formation of intermetallic compounds within the interfacial region. The films and the interfacial regions were characterized through x-ray photoelectron spectroscopy and the resulting h_{BD} values were measured with time-domain thermoreflectance. The thermal boundary conductance values were directly correlated to the size of the interfacial region and the thermal boundary conductance could be enhanced by up to 60%. The thermal boundary conductance values were also dependent upon the transition rate and phase composition of the transition layer. Overall, the results support that the thermal boundary conductance can be enhanced by promoting a compositionally-mixed gradient at the interface. Utilizing purposeful mixing layers at an interface remains a promising avenue for controlling the thermal boundary conductance at alloy/semiconductor interfaces ubiquitous in microelectronic devices.

(1) J.L. Smoyer, PhD Thesis, University of Virginia (2015).
(2) R. Rastgar, et al., *Nanoscale*, 13, pp. 6254- 6262. (2019).

Concept of self-phased elements in reflectarray and transmitarray antenna

Quang M. Nguyen, *Amir I. Zaghloul*, FCDD-RLS -RR

Antennas are key elements in Army communication systems, with the main function of the generation, transmission, and propagation of modulated electromagnetic (EM) waves. Among different types of antenna, the reflectarray and transmitarray antenna have received considerable attention in the RF community due to high-gain, broadband, light-weight, and low-cost. Compared to traditional phased array antenna, their spatial feeding method does not suffer the insertion loss of a feed network. Instead, the desired phase shift from each element can be obtained by tuning the dimensions of the element around its resonant size. This approach also results in fixing the direction of the main beam, which substantially limits the applications of the reflectarray and transmitarray antenna in the Army.

In this work, we propose a concept of self-phased elements used in the reflectarray and transmitarray antenna. Since each antenna element has self-phasing capability, this would enable beam-steerable in the array system. Self-phasing results from dynamically controlling the effective permittivity of the antenna substrate. We explore tuneable dielectric substrates by applying a DC bias to the material. A DC bias introduces a current that can alter a dielectric's electrical properties. We incorporate the use of meandering line or inter-digitated concepts into the design to increase the effective aperture while still achieving a sub-wavelength element design ($\lambda_0/4$ - $\lambda_0/6$). The new design element is more compact than the element used in the conventional reflectarray and transmittarray antenna designs, which are typically a half-wavelength ($\lambda_0/2$) in dimension at the center frequency of the band of operation. Depending on the criteria, the element may be configured in stacked layers to achieve the full 360^o tuneable phase range.

Photoelectrochemistry of III-V epitaxial layers and nanowires for solar energy conversion

Vijay Parameshwaran, FCDD-RLS-CC

III-V materials, which exhibit high absorption coefficients and charge carrier mobility, are ideal templates for solar energy conversion applications. Historically, their use has been limited to multijunction stacks for high-efficiency and high-cost concentrator photovoltaics. Recent research has explored utilizing epitaxial III-V crystals as light absorbers for driving a variety of chemical reactions to generate hydrogen and hydrocarbons as fuels. The ability to grow single crystal nanowire morphologies of these materials opens up the design space to obtain higher efficiency electrodes and stand-alone photocatalysts that utilize less materials for consumption. A basis in development of III-V layers and nanomaterials for solar-driven chemical reactions is the junction between the semiconductor and the electrolyte.

This work describes the photoelectrochemistry research in several III-V/electrolyte junctions as an enabler for device design for solar chemical reactions. Epitaxial phosphide layers are grown on silicon and GaAs to show an extended space charge design to improve the quantum efficiency of heterojunction photocathodes (1). Studies on microstructured and nanostructured forms of GaN show insights to how morphology determines the nature of the electrochemical junction (2). Electrochemical photoeffects on both InP and InN nanowires provide a basis on how nanostructured forms of these semiconductors can be engineered for solar fuels while providing fundamentals on the interface (3). The nanowire engineering has also extended to the GaP nanowires, grown on both silicon and GaAs. Finally, work

on integrating GaAs nanowires with ALD nickel oxide catalysts has led to the first demonstration of OER in this materials system (4).

V. Parameshwaran et al., *Journal of the Electrochemical Society*, 163 (8), pg. H714-H721 (2016).
V. Parameshwaran et al., *Journal of the Electrochemical Society*, 163 (10), pg. H958-H963 (2016).
V. Parameshwaran et al., *ACS Applied Materials and Interfaces*, 8 (33), pg. 21454-21464 (2016).
J. Zeng, V. Parameshwaran, X. Xu et al,, *Journal of Electronic Materials*, 47(2), pg. 932-937 (2018).

Porous Silicon inks for safely 3D printed explosive structures

Kate Price, *Philip M. Guerieri*, *Wayne A. Churaman*, FCDD-RLS-EM

Emerging additive manufacturing technologies have the potential to drastically modify fabrication of energetic systems in military applications. Rapid prototyping, spatially graduated material properties, and cost effective structure-function controls in printed propellants and explosives are driving rapid feedstock and ink formulation research, especially using experimental nanoscale reactive ingredients including nanothermites. At the nanoscale high specific surface area can facilitate extreme interfacial mixing of fuel and oxidizer components required for particle composite energetics to reach reaction rates relevant to propellants or even explosives. However, metal fuel nanoparticles including aluminum and boron continue to react in such formulations too slow to participate in explosive detonations due to native oxide passivation layers and nanoscale powders pose significant safety hazards. Microparticles of porous silicon (PS) featuring nanoscale porosity offers a fuel alternative at or exceeding the specific surface area of nanoscale powders for safer handling. Hydrogen termination on silicon also replaces native oxide passivation with an energetic surface chemistry for high active silicon content. This work describes recent efforts for fabricate PS feedstocks and formulate 3D printing inks for deposition of polymer bound PS particle structures. A unique benefit of existing on-chip energetic PS is maintained with this print method: the material is deposited without an oxidizer component in a safe non-reactive form. After drying, an activation solution with sodium perchlorate oxidizer can be applied to infiltrate the structure at the nanoscale within PS pores and react with flame speeds exceeding 1 km/s. This work has the potential to replace primary explosives in igniters and initiators with a scalable cost-effective

alternative suitable for MEMS integration and unparalleled performance tuning by formulation and structure.

Synthesis and characterization of novel, broadband nonlinear-absorbing chromophores

Thomas N. Rohrabaugh, Jr., *Ryan M. O'Donnell*, *Trenton R. Ensley*, *Michael J. Ferry*, and *William*
M. Shensky III, FCDD-RLS-RL

Due to their tunable photoreactivity and light absorbing properties, organometallic iridium(III) complexes have a wide variety of applications such as phosphorescent dopants in organic light emitting diodes (OLEDs), chemical sensing, light harvesting for solar cells, and photodynamic therapy. Particularly, our team is interested in their non-linear optical (NLO) properties such as reverse saturable absorption (RSA) and two-photon absorption (2PA). Our objective is to utilize the *ARL RSA Material Development Loop* to design, synthesize, and characterize organometallic iridium(III) complexes that exhibit panchromatic absorption in the ground state and excited state, resulting in panchromatic RSA agents. The methodology for material design and an example of a series of iridium(III) complexes, structure $[Ir^{III}(C\wedge N)_2(acac)]^0$ (where acac = acetylacetonate and C∧N = 2-phenylquinoline, 2,4-diphenylquinoline, 6-nitro-2-phenylquinoline, or 6-nitro-2,4- diphenylquinoline) will be discussed in detail herein.

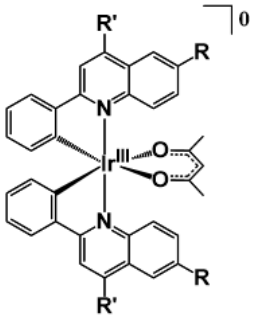

R = H or NO_2
R' = H or Ph

High speed detection characterization of event-based sensors

Jonah Sengupta, *Benjamin Linne*, RDRL-WMP-D

Event-based sensors have demonstrated latencies on the scale of 1-10 microseconds making the technology an energy-efficient, lightweight option for real-time, high speed object detection and tracking. Research has been conducted to characterize the sensor's abilities to detect high-speed objects in a controlled-environment to

establish performance upper limits and induce what on-chip channels and physical mechanisms act as bottlenecks. A configurable LED strip with user interface was designed and implemented to extract this detection cutoff in a lab-controlled environment. Since the event-based sensor responds to changes in intensity, switching on individual LEDs consecutively simulates the effect of an object moving across its field of view. A user-interface was embedded into the LED strip to allow for customization of the simulated projectile's "velocity". After calibrating the sensor, the detection limit was systematically extracted by increasing this velocity from 50 to 1000 m/s in rough increments. Using a custom signal processing algorithm, the location of the projectile tip was extracted. By tracking the number of average tip positions over the range of recorded shot velocities, linear extrapolation shows the absolute limit of the event-based sensor to be 1450 m/s. Faster speeds and more recordings can be used to verify this conclusion.

Data encoding for information camouflage to improve C2 decision-Making in multi-domain environment

Piyush K Sharma, FCDD-RLC-IB

The military is investigating methods to improve communication and agility of networks in its multi-domain operations (MDO). Nascent popularity of Internet of Things (IoT) has gained traction in public and government domains. Its usage in MDO may revolutionize future battlefields and may enable strategic advantage. While this technology offers leverage to military capabilities, it comes with several challenges with increased uncertainty and security risk. A key question is how to address these uncertainties? Recently published studies proposed information camouflage technique to transform information from one data domain to other. As this is comparatively a new approach, we investigate challenges of such transformations and the associated uncertainties, specifically unknown-unknowns to improve decision-making.

Solid state power emulator to evaluate $\frac{1}{2}$ H-Bridge Module

Richard Thomas, FCDD-RLS-DP

The next step beyond single device evaluation is the evaluation of multiple devices or modules used to enable operation of high power motors, inverters and converters. The challenge with testing multiple devices is the increased power supply and load capacity required for proper evaluation. To evaluate multiple MOSFET's in the $\frac{1}{2}$ H-bridge circuit configuration running at 600V, 50A at 10kHz with an on-time no less than 80% under normal testing conditions would require a 30kW power supply

and a load to handle such power. To significantly reduce the needed power supply and load to handle this evaluation the Solid State Power Emulator (SSPE) underwent an upgrade from testing a single device to testing a $\frac{1}{2}$ H-bridge circuit. Using this upgraded SSPE for the $\frac{1}{2}$ H-bridge evaluation, the testing only requires ~5 kW power supply which is approximately an 83% power savings. The goal of this research is to compare and evaluate different devices, their heat management and analog testing for low inductance 3 phase AC motors.

α-Sn Magnetotransport devices

Owen Vail, *Patrick Folkes, Patrick Taylor, George de Coster*, FCDD-RLS-DE

The large spin-orbit coupling of diamond-cubic α-Sn shows great promise for magnetic memory devices along with its topological band structure and single-element nature. As such, consistent high-quality growth on insulating CdTe opens the doors to unconventional electronics using a widely available source material. After verifying epitaxial growth of our films, we perform transport measurements to characterize the electronic carriers in the material. We identify two-channel transport and semimetallic behavior in thicker samples, while thinner samples that approach the topological insulator regime are dominated by impurities resulting from the particulars of growth on the CdTe substrate. We apply a field effect gate voltage in order to modulate the channel between majority n-type and majority p-type carriers and further characterize its behavior under large magnetic fields. Careful preparation of the CdTe surface before growth is considered crucial to attain a low residual density and accessible topological states on an insulating substrate. This work readily lends itself to the development of topologically enabled devices for fieldable applications such as low power magnetoelectronics.

Toward optical interfaces for quantum networks: Characterization of optical coupling between SNAP microresonators and tapered optical fibers

Dashiell L. P. Vitullo, FCDD-RLC-NT

Quantum information networks offer fundamentally novel information processing and distribution capabilities with potential applications including secure communications and distributed sensing. Quantum light can be viewed as a resource for communicating quantum information through- out such networks, but its fragility is a major challenge. New equipment capable of routing and storing quantum light without losing or breaking it must be developed. Optical microresonators are a promising platform for routing and storing quantum light, as they offer ultra-low loss and high-efficiency interfacing between existing low-loss

optical fiber networks and sources of quantum light (e.g. atoms, nonlinear optics). The surface nanoscale axial photonics (SNAP) platform in particular boasts sub-angstrom fabrication precision and demonstrated slow tunability. To develop minimal-loss systems, a characterization scheme that measures and validates the loss and coupling strength between a microresonator and an optical fiber is required. Here, we review our methodology for robust partially-automated characterization of evanescent optical coupling between a SNAP microresonator and a tapered optical fiber, and describe our vision of utilization of fast all-optical microresonator control to realize optical interfaces in quantum networks.

Phonon transparency at high interface density of nanolaminate thin films

Adam A. Wilson[1], *Darin J. Sharrar*[1], *Ronald Warzoha*[2], *Andrew Smith*[2]
[1] FCDD-RLS-DP, [2] Dept. of Mechanical Engineering, US Naval Academy

Interface thermal resistance contributes significantly to the overall thermal resistance experienced in electronic devices and packages. The ability to manipulate thermal resistance at interfaces is paramount to the development of electronics relevant to the Army, which are constantly in pursuit of electronics capable of delivering more power at faster switching speeds. On the opposite side of the thermal spectrum, temperature detection is a critical domain that relies on strong changes in temperature with small heat inputs, which corresponds with high thermal resistance. Therefore, if thermal resistance can be tailored by simply adding material interfaces from the same materials that are typically used in sensors, thermal resistance can be increased and sensitivity of the detector can be enhanced. In this study, we report the effect of increased interface density on the measured effective thermal conductivity of nanolaminate thin films, compare with a semi-analytical diffuse mismatch model (DMM), and discuss the effect of phonon transparency on how heat propagates across heterogeneous material interfaces. It is determined that at interface densities above 10 μm^{-1}, thermal resistance begins to deviate significantly from the DMM predictions, but that experimentally measured effective thermal conductivity at 100 μm^{-1} is >2.5× reduced compared with the case where interface thermal resistance plays no role in the measured effective thermal conductivity (1.08±0.06 $Wm^{-1}K^{-1}$ vs 2.63± 0.11 $Wm^{-1}K^{-1}$), but is still much larger than the value predicted by DMM (0.44 $Wm^{-1}K^{-1}$). The insights of this study are useful to tailor thermal properties of devices on both the high thermal conductance and low thermal conductance side.

Antibody-Recruiting protein-catalyzed capture agents as a therapeutic for COVID19

Alexander Winton[1], *Matthew Coppock*[1], *Sanchao Liu*[1], *Bert T. Lai*[2], *Anders Eliasen*[2], *Matthew N. Idso*[3], *James P. Hopkins Jr.*[3], *Sanchao Liu*[1], *Jessica Yee*[3], *Sunga Hong*[3], *Rachel Calder*[3], Katrine Museth[2], *Fred Mast*[4], *Heather Agnew*[2], *Michael Klimas*[2], *James R. Heath*[3]

[1]FCDD-RLS-CB, [2]Indi Molecular, Inc., Culver City, CA, [3]Institute for Systems Biology, Seattle, WA, [4] Center for Global Infectious Disease Research, Seattle Children's Research Institute, Seattle, WA

Protein Catalyzed Capture (PCC) agent research is currently pursued at ARL as an alternative to state-of-the-art antibody recognition elements for sensor applications, as these agents address gaps in discovery time, batch-to-batch variation, and cost effective and scalable manufacturability. The current Covid19 project strives to demonstrate the untapped versatility of PCC agents, where discovered recognition elements may be employed beyond detection applications, as a therapeutic to treat an emerging disease threat. By making modular modifications to PCC sensing elements (addition of a hapten moiety) a therapeutic may be rapidly developed (in tandem with a sensing element), capable of recruiting a person's endogenous antibodies to aid in clearing foreign pathogens.

Structural analysis and bioinformatics were employed to guide the development of target epitopes from the spike protein of SARS-CoV-2 and were then screened against cyclic peptide libraries where PCCs were identified by un-catalyzed, in situ "click" chemistry. PCC affinities for the SARS-CoV-2 Spike protein were validated by high-throughput assay screening and most promising PCCs were modified and shown to exhibit antibody recruitment ability. Further PCC studies seek to characterize the solution affinity of these agents relative to surface bound affinities, while In vivo testing of affinity matured AR-PCCs in animal models is currently in progress. The rapid screening and maturation process of AR-PCCs depicted in this work demonstrates the capability of this technology to enable Army capabilities for a rapid and robust pandemic response.

Thermoforming process model for thermoplastic composite parts

Michael Yeager, FCDD-RLW-MA

Ultra-high molecular weight polyethylene (UHMWPE) has increasingly been utilized for ballistic protection due to its high strength to weight ratio. Commercially available UHMWPE usually consists of aligned fibers or films embedded in a thermoplastic polymer matrix. When manufacturing complex curvature parts, the flat sheets of material undergo a thermoforming process before

undergoing high pressure consolidation between matched metal tooling. In the thermoforming process, the material is punched through a die plate at a low displacement rate while a binder plate applies an out of plane constraint. The in-plane shear response of the UHMWPE is a critical input for the numerical simulation of this process as it will dictate how easily the material conforms to the complex curvature shape. A characterization methodology is developed to characterize the non-linear in-plane shear response of UHMWPE from a simple tensile test. The in-plane shear response is input into a numerical model to describe deformation during preforming. Modeling each individual sheet of UHMWPE is not computationally efficient, leading to the development of a methodology to scale the number of sheets modeled in each layer within the model. The scaling methodology is validated experimentally and its limits are evaluated. The model is exercised to explore the influence of in-plane shear constitutive response on final preform thickness.

Appendix B. Contributed Posters Presented at the 5th Postdoc and Early Career Research Day

The contents of this appendix appear in original form, without editorial change.

Laser Formed Compliant Mechanisms

Project Objective Statement

Design, model, and test ve basic compliant mechanisms created with laser forming to determine the validitiy of the method and the design space for manufacture.

Current Art

Laser Forming: The process of bending sheet metal through heating with a laser in such a way that de ned sections crease and fold. Rigid structures have been created.

Compliant Mechanisms: Flexible mechanisms in mechanical systems that are designed to replace traditional mechanical components and joints. Never before created with laser forming.

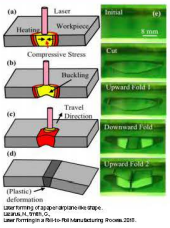

Applications

Complinat mechanisms manufactured with laser forming are useful for rapid prototyping, replacing rigid components, achieving difficult geometries, conductive flexible structures, etc.

Army applications:
- Antennas
- Fuzing
- Armaments
- Sensors
- Smart Devices

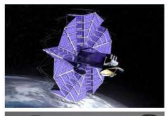

Compliant Solar Array and Rocket Thruster Actuator
BYU Compliant Mechanisms Research Lab

Mechanisms

Parallel-guided Mechanism

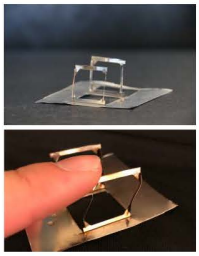

The negative space is laser cut and removed. The compliant members are folded perpendicular to the sheet. The mechanisms are then folded out-of-plane.

Split-tube Flexure

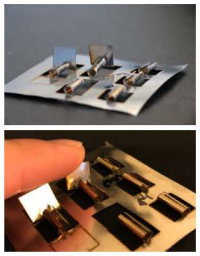

The laser-formed split tube flexure is folded one segment at a time 0.625mm apart until a cylindrical shape is formed.

Bi-stable Switch

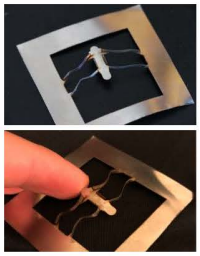

The negative space is laser cut and removed. The compliant members are folded perpendicular to the sheet. The shuttle can be actuated between two stable states.

LET Joint Array

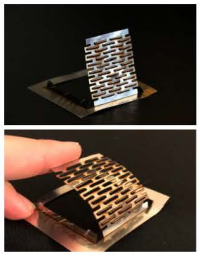

The negative space is laser cut except for flaps that are folded out-of-plane. The flaps promote stiffness against undesired motion while allowing bending of the array to be retained.

Cross-axis Flexural Pivot

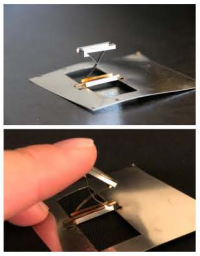

The laser-formed cross-axis flexural pivot is created out of two mirrored patterns. The compliant members are folded perpendicular out-of-plane and then the two sides are folded up to join each other.

Daniel C. Ames - Brigham Young University
Gabe Smith, Nathan Lazarus - ARL
September 2020

A GAME THEORETIC FRAMEWORK FOR SOFTWARE DIVERSITY FOR NETWORK SECURITY

By: Ahmed Hemida, Nandi Leslie, Charles Kamhoua

Motivation

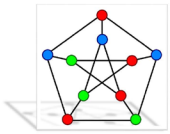

System Model

- Each node represents a host.
- The network represented as a graph.
- Software diversity over graph is a graph coloring problem.
- A graph coloring outcome can be effective in diversity for a given number of colors.
- Colors : Are the number of software types.

Defender Model

- The defender does not allocate the available resources.
- The defender decides the number of resources (# of colors).
- The defender tradeoff:
  - Increase the level of diversity via increasing the number of software types.
  - The cost of diversity increases as well.
- The reward of diversity is quantified through the diameter of graphs.

$$NV = NSW \times SWV.$$

$$NSW = \begin{bmatrix} 1 & 0 \\ 0 & 1 \\ 0 & 1 \end{bmatrix}$$

Graph coloring output

Available information

Attacker Model

The goal of the attacker is to compromise a subset of targeted nodes.

Attacker has a set of probes to compromise a set of vulnerabilities.

There is a cost associated with each probe.

$$\mathbf{P} = \begin{bmatrix} 1 & 0 & 0 \\ 0 & 1 & 1 \end{bmatrix}$$

The attacker trade-off:

Attack the network using a larger number of probes to compromise more nodes

Reducing his attack cost to avoid expensive attacks.

Game Model

- The defender payoff function: $K = mean\left(\sum_{v \in \mathcal{N}} \left(\sum_{u \in \mathcal{P}_v} \mathbb{1}_{\{u \in \mathcal{E}(a_2)\}}\right)\right)$

$$R_1(a_1, a_2) = -K - C_d(a_1),$$

Average number of reachable nodes

Diversity cost

- The attacker payoff function:

$$R_2(a_1, a_2) = K - C_a(a_2).$$

Attack cost

Algorithm

Algorithm 1 Diversify

```
procedure DIVERSIFY(G, S, B, SWV, P, C_d, C_a)        ▷ Input parameters
    System Initialization
    Define: A_1, A_2
    for a_1 ∈ A_1 do
        Graph Color (G, a_1)                          ▷ Graph coloring algorithm
        Update NSW                                    ▷ Build node-software matrix
        Compute NV = NSW × SWV                        ▷ node-vulnerability matrix
        for a_2 ∈ A_2 do
            Compute R_1(a_1, a_2) → update A
            Compute R_2(a_1, a_2) → update B
    GameSolver(A, B) → x*, y*                         ▷ Mixed strategies equilibrium for (7),(8)
```

Results

Effect of number of software types:

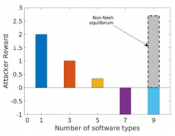

(a) Attacker reward.

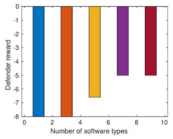

(b) Defender reward.

Effect of action cost:

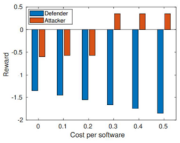

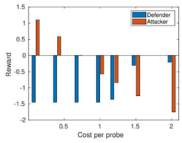

Complexity reduction:

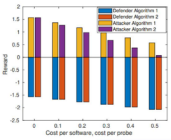

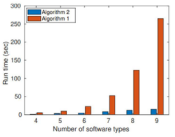

Conclusion

- Developed a novel game model to study:
  The interactions between network defender and an adversary when software diversity is the main defensive strategy for the defender.
- Exploit graph-coloring algorithm for deploying Nash equilibrium diversifying strategy over graphs.
- Proposed a complexity reduction approach to obtain Nash equilibrium for large scale networks with a larger number of colors

A TOOLKIT FOR ASSESSING COMMUNICATION IN HUMAN-AUTONOMY TEAMS

Anthony L. Baker, Daniel E. Forster, Catherine Neubauer, Sean M. Fitzhugh, Andrea Krausman and Kristin E. Schaefer
U.S. Army CCDC Army Research Laboratory

This poster describes four novel communication-based approaches for explaining trust, cohesion, and performance in human-autonomy teams: 1) aggregate communication flow; 2) relational event modeling; 3) linguistic similarity; and 4) facial expression analyses. These approaches can be used to understand when team trust or cohesion break down during interactions with autonomy and can be used to identify when critical interventions are necessary to appropriately calibrate trust and cohesion. This work supports the Human-Autonomy Teaming Essential Research Program, the Wingman Joint Capabilities Technology Demonstration, and the Next Generation Combat Vehicle modernization priority. *References provided on this PowerPoint's Notes

Aggregate Communication Flow

Overview

This approach analyzes how much communication occurs between each pair of senders and recipients in a team. Different flow patterns can be used to adapt training to improve team effectiveness.

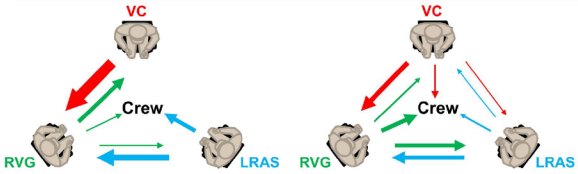

Army Crew, 2018
Gunnery Score: 563/700

Marine Crew, 2019
Gunnery Score: 308/700

HAT Keys

- Can be computed using spoken exchanges or text chat.
- With correct setup, flow can be captured real-time based on button presses or mic detection.
- Approach is flexible to complex human-autonomy team structures, but doesn't consider time order of interactions

Relational Event Modeling

Overview

REM is a model-based approach for analyzing dynamic networks. It leverages information embedded in the timing of interactions to model interaction rates as a function of prior communication and individual attributes.

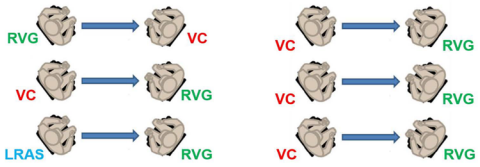

Order & timing of interactions provide detailed team dynamics

REM identifies patterns such as inertia

HAT Keys

- Highly flexible to team interaction modalities
- Self-reported trust data can be used as individual attributes to model one's propensity to send or receive interactions
- Model coefficients be used to identify links between network dynamics and group-level trust measures

Linguistic Similarity

Overview

This approach uses the content of communication to understand how lexical and syntactic patterns explain team processes. It can track human synchrony as well as inform how autonomy could adapt communication.

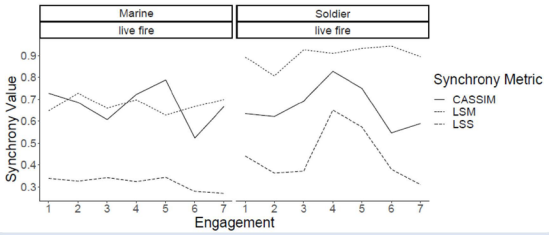

HAT Keys

- Characterizes how quickly, and how well, team members form a common communication style.
- Can analyze verbal and non-verbal communication, allowing for direct application to human-autonomy teams
- Requires accurate transcriptions of communication.

Facial Feature Analysis

Overview

This analysis detects emotional states using facial features. Facial expression calculations are based on single Action Unit (AU) evidence which can be grouped to reveal changes in universal emotions.

Facial expression Action Units

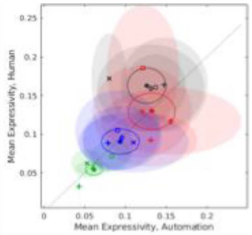

HAT Keys

- Noninvasive and can be used to supplement other subjective or physiological modalities
- Can be analyzed real-time or offline depending on software
- Changes in emotions during specific teaming scenarios can indicate changes in affect-based trust

Path Forward

These approaches are critical to understanding human-autonomy teams because they can be utilized **unobtrusively** and **continuously** to explain and improve team effectiveness. Future work will refine our multi-method approach for assessing team trust and cohesion, and improve our understanding of how communication patterns relate to team effectiveness in different team structures and contexts.

This research was supported in part by an appointment to the US Army Research Postdoctoral Fellowship Program administered by the Oak Ridge Associated Universities through a cooperative agreement with the US Army Research Laboratory (ARL). Research was sponsored by ARL and was accomplished under Cooperative Agreement Number W911NF-18-2-0230

5th Annual Postdoc Research Symposium, Sep 2020

Deceptive Maneuver in Multi-Domain Operations (MDO) using Multi-Agent Reinforcement Learning (MARL) to Gain Superiority Over the Adversary

Anjon (Sunny) Basak & Derrik E. Asher
US CCDC Army Research Laboratory, CISD-ISD-CUB

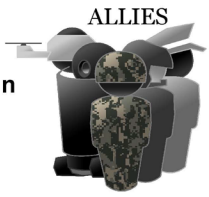

Problem

- **Degraded superiority** in multiple domains.
- Enemy *fractures* AirLand Battle by countering **predictable use** of domain fettered approaches.
- Advancement of urbanization, **near peer states compete below armed conflict**.
- Adversaries create **tactical, operational and strategic stand-offs**.

Conventional AI Problems:

- Noisy and scarce data for training AI models.
- Not robust enough to handle unseen examples.
- Too much computational power required for training.
- Integration of heterogeneous agents.

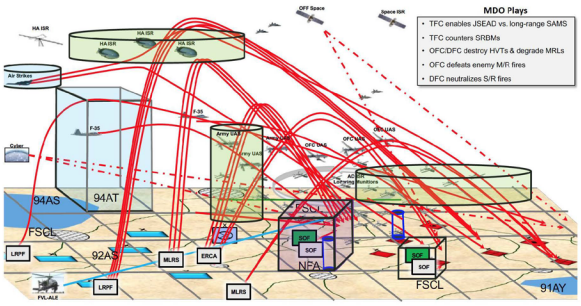

Exemplar Internet of Battlefield Things (IOBT) Scenario Implementing the MDO Effect Loop

[1] Abdelzaher, T., Taliaferro, A., Sullivan, P., & Russell, S. (2020, May). The Multi-Domain Operations Effect Loop: From Future Concepts to Research Challenges. In Artificial Intelligence and Machine Learning for Multi-Domain Operations Applications II (Vol. 11413, p. 1141304). International Society for Optics and Photonics.

Research Goals

- Becoming less obvious to the eye of the enemy in Multi-Domain Operations (MDO).
- Using **collaborative deception** to manipulate, learn, deter and exploit the adversary.
- Using deception to improve the integration of capabilities: converge.
- Thinking ahead what the adversary would do and act based on the prediction to be resilient
- Heterogeneous agents working together: **collaborative deception**.
- Inexperienced Soldiers need to easily, seamlessly, and intuitively interact with AI teammates so that survivability and Mission goals are not compromised.

Technical Approach

- Extending existing tasks to incorporate deception and MDO capabilities.
- The Multi-Agent Deep Deterministic Policy Gradient (MADDPG) algorithm does not scale to a large number of agents and is not robust to sudden behavioral changes in agents (e.g., external agents are introduced).
- Decomposition of the Q-value function in the MADDPG algorithm into independent components to handle different components of complex tasks (e.g., Combined Arms Breach).
- Incorporating model-based reinforcement learning (RL) in MADDPG to be more robust to handle unseen examples and to improve efficiency (reduce the down time). For example; Dyna-Q+.
- Using simulation based approach to make predictions more efficient rather than solving the whole MDP (e.g., MCTS & Dyna-2 approaches).
- Integrating human state into the Q-value of agents.

Predator-Prey Pursuit

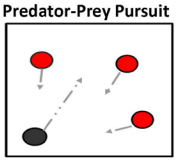

Predator Prey

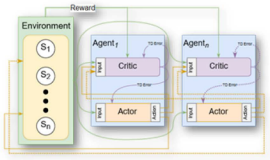

Multi-Agent Deep Deterministic Policy Gradient (MADDPG)[1]

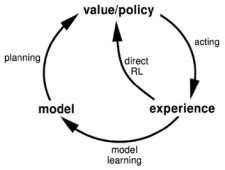

Integration of model-free and model-based approach

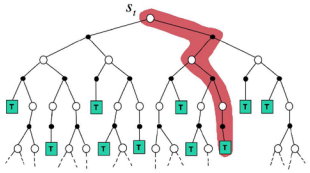

Simulation based approach

[2] Lowe, Ryan, et al. "Multi-agent actor-critic for mixed cooperative-competitive environments." Advances in Neural Information Processing Systems. 2017.
[3] Zaroukian, Erin, et al. "Algorithmically identifying strategies in multi-agent game-theoretic environments." *Artificial Intelligence and Machine Learning for Multi-Domain Operations Applications*. Vol. 11006. International Society for Optics and Photonics, 2019.
[4] David Silver, Online RL Lectures Slides.

Without deception

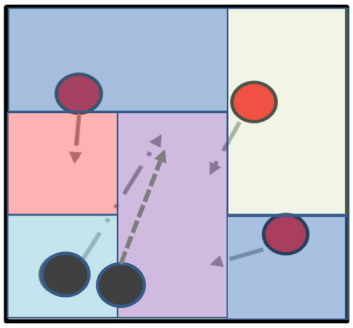

Predator Prey

With deception

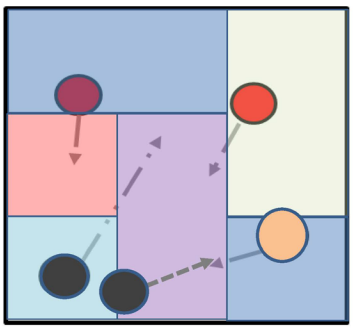

Predator Prey

Introducing enemy friendly entity(deception)

Deception

- **Visual**: radar, 3D image from satellite **Auditory**: mimicking noise
- To enforce the enemy to allocate resources somewhere else. **Injecting false** sounds in enemy's communication. Social, Economical, etc.

Purpose of deception:

- **Distract, deter, lure, exploit, signal, learn, converge.**
- **Manipulate**: make such a move which reveals maximum information by enemy action.
- **Camouflage, cut down.**

Contact Information
US CCDC ARL
Derrik E. Asher, PhD
Computational Psychologist
derrik.e.asher.civ@mail.mil

UNCLASSIFIED

RAGNAROC: A computational tool to understand how attentional mechanisms will respond to augmented reality displays

Chloe Callahan-Flintoft, Michael Geuss, & Gabriella Brick Larkin
US Army Research Lab

A problem to solve

- AR displays can alert Soldiers to targets in their visual field
- The goal is to improve response times to target while still allowing Soldiers autonomy to survey the environment

How can we guide a Soldier's attention without damaging their situational awareness?

- Attentional capture is the phenomenon where reaction times to a target are slower when a highly salient, though task-irrelevant, distractor is present (Theeuwes, 1994)

- However attentional capture can be overcome as studies show the visual system's ability to suppress the salient distractor and successfully allocate attention to the target (Gaspelin, Leonard, & Luck, 2015)

When does attentional capture happen?

RAGNAROC

- The **R**eflexive **A**ttention **G**radient through **N**eural **AtR**act**O**r **C**ompetition model is a rate coded neural network using O'Reilly & Munakata (2001) equations to simulate membrane potential

$$MP_{i,j,t} = MP_{i,j,t-1} + dtV_j \times [(Bias_j + Excite_{i,j,t-1}) \times (EE_j - MP_{i,j,t-1}) + Inhib_{i,j,t-1} \times (EI_j - MP_{i,j,t-1}) + Leak_j \times (EL_j - MP_{i,j,t-1})]$$

Attention Map:
- Aggregates input
- Mediates competition

Late Visual:
- Differentiates stimuli
- Permits top-down control

Early Visual:
- Represents initial input

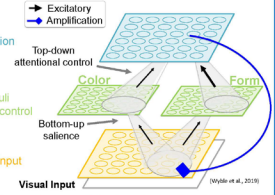

How does the model simulate data?

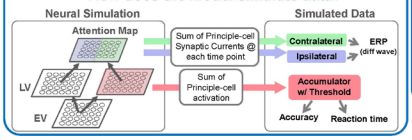

What are 'targets' and 'distractors'?

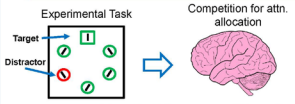

How is this competition decided?

Attentional Priority = Visual Salience * Task Relevance

Attentional priority scale:

- This moves attention out of the laboratory dichotomy of targets & distractors and into a more flexible, real-world spectrum where stimuli vary in both saliency and task relevancy

How is attention allocated?

- In RAGNAROC all maps are spatiotopically organized
- Attention enhances processing at a certain **location** rather than of a certain stimulus

How does attention inhibit processing?

Surround inhibition:

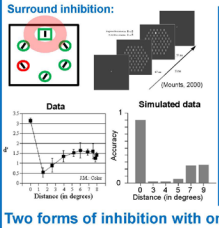

Selective inhibition:

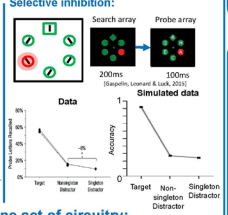

Two forms of inhibition with one set of circuitry:

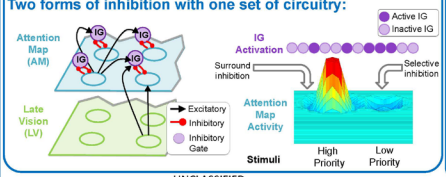

Attn. control settings' effect on capture

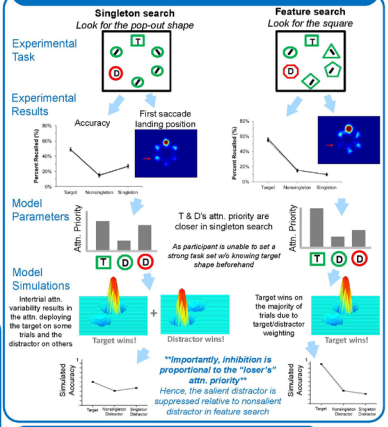

Model predictions & applications

- Augmented Target Recognition (ATR) could aid soldiers in the field by highlighting potential threats
- ATR systems must guide attn. resources while maintaining user autonomy and situational awareness (i.e. avoid capture or effective blindspots due to attn. suppression)

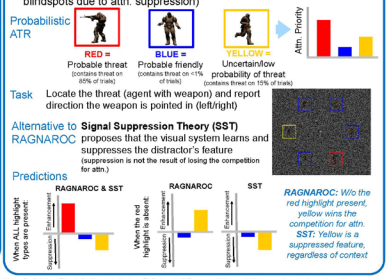

Wyble, B., Callahan-Flintoft, C., Chen, H., Marinov, T., Sarkar, A., & Bowman, H. (in press). Understanding visual attention with RAGNAROC: A Reflexive Attention Gradient through Neural AttRactOr Competition. *Psychological Review*.

UNCLASSIFIED

UNCLASSIFIED

Development of Michael Addition Binder System for Additive Manufacturing of Energetic Materials

Anthony M. Clay[1,2], Joshua R. Mitchell[2], David M. VanOosten[2], Ian M. McAninch[2], John J. La Scala[3], E. Jason Robinette[4]

1. anthony.m.clay10.civ@mail.mil; 2. FCDD-RLW-MD; 3. FCDD-RLW-M; 4. FCDD-RLW-D

Objectives

1. **Safely print high energy formulations**
   - High solids loadings of energetic materials (HMX/RDX)
   - Energetic binders
2. **Manufacture relevant geometries**
   - Printing high viscosity pastes with resolution < 100 µm
3. **Maintain or increase grain performance**
   - Mechanical properties to withstand high g forces
   - Enhanced combustion

Method

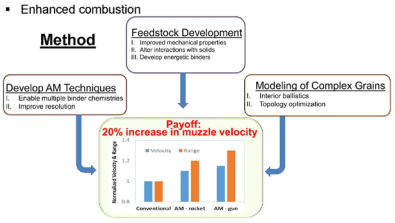

10% more muzzle velocity ≈ 80 s engagement advantage or 10 – 15 rounds unopposed

Additive Manufacturing of Energetic Material Opportunities:

Novel geometries for gun propellant

i. Controlled burn rate
ii. Tailored progressivity
iii. Increased muzzle velocity

Figure 1: Example of perforated propellant geometries plausible with AM.

Graded prints for rocket propellants to tailor progressivity.

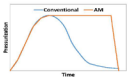

Multi-material prints or composite energetic material (eg. explosives)

i. Multi-point ignition
ii. Imbedded ignition
iii. Increased loading density of energetic particles
iv. Packed grains → monolithic charge

AM of energetic materials has the possibility of being a disruptive technology by offering the capability of increased range, controlled energy release and an overall increase in energy.

Develop AM Technologies: Ambient Reactive Extrusion (ARE)

Ambient Reactive Extrusion allows for the deposition of reactive components that gel fast enough to build sufficient green strength to allow continuous printing yet cures slow enough to all crosslinking between layers.

- Two-part resin direct ink write (DIW) AM methodology
- Can tolerate difference in viscosity between separate reservoirs
- Can tolerate high viscosity materials
- Can tolerate particulate solids
- Easy to incorporate energetic materials
- No need for elevated temperatures
- Highly scalable

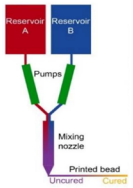

Feedstock Development for ARE: aza-Michael Addition (A-MA)

Benefits of Michael Addition

+Thermodynamically Favored
+ Atom Economic
+ No unwanted byproducts
+ High Conversions
+ High yielding
+ Commercial available
+ Low toxicity

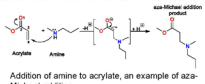

Addition of amine to acrylate, an example of aza-Michael addition

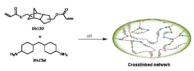

Crosslinking possible via formed secondary amines

Rigid Elastomeric

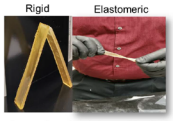

Thermosets produced of cross-linked A-MA networks

- Can obtain T_gs ranging from -40 °C to 46 °C.
- Can gel at ambient conditions
- Gel times less than 2 minutes
- Can tailor polymer properties (ie. glassy vs elastomeric)

Compounds used in this investigation

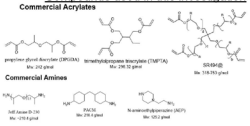

ARE 3d printed cylinder of Formulation 8.

- 30 mm height
- 12 mm diameter perforation
- ~45 wt% solids loaded
- Able to print high viscosity component PAM 2 of > 88,500 cPs!

UNCLASSIFIED

Feedstock Development Cont'd.

Table 1: Tgs based on DSC and qualitative properties of A-MA thermosets

Formulation	Acrylate	Amine	Molar Ratio (Ac:NH)	Tg (° C)	Qualitative Flexibility	Gel Time
1	DPGDA	D230	1:1.34	-32	Moderate	Does not gel
2	DPGDA	PACM	1:1.34	-11	Low	Does not gel
3	TMPTA	D230	1:1.2	-12	Low	>3 h
4	TMPTA	AEP	1:0.9	31	Stiff glassy material	25 s
5	SR494@	D230	1:0.9	-17	Moderate	2h 30 min
6	SR494@	PACM	1:0.9	13	Low	14 min

Structure property relationship established and used to develop printable formulation 8.

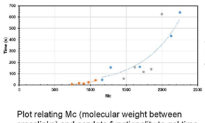

Plot relating Mc (molecular weight between crosslinks) and acrylate functionality to gel time. Amines of differing mw and acrylates of different functionality and mw.

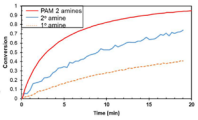

Kinetics of amines reacting with SR494@ obtained from NIR.

Increased acrylate functionality and amine substitution alters gel times!

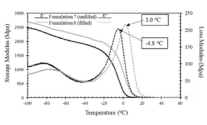

DMA results of ARE amine PAM 2 formulations.

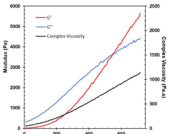

Rheological Properties of SR494@ and PAM 2

Can relate gel times, to structure of amine, acrylate functionality and rheological properties to aid in developing ARE printing parameters.

Table 2: Properties of printable A-MA thermosets.

Formulation	Acrylate	Amine	Solids Loading (wt. %)	E' @ -40° C (Mpa)	E'' Tg (° C)	DSC Tg (° C)	Gel time (s)
7	SR494@	PAM 2	0	2300 ± 500	-4.8	-5	90 ± 15
8[2]	SR494@	PAM 2	~45	2300 ± 300	3.0	n/a	120 ± 15

Summary

- Successfully printed A-MA formulation on ARE
- Achieved solids loading of ~45 wt.% of glass

Future Efforts

- Lower Tg (near – 30°C)
- Determine stability of ARE formulation with energetic solids
- Print ARE A-MA formulation with energetic solids

UNCLASSIFIED

Reconstruction of Prior Austenite in High-strength Wrought and L-PBF Processed AF9628 Steel

S. Cluff[1], A. Kudzal[1], D. Field[1], E. Vasilev[2], V. Sinha[3]
Email: stephen.r.cluff2.civ@mail.mil

[1]Army Research Laboratory, FCDD-RLW, Aberdeen Proving Ground, MD, 21005, USA
[2]Department of Mechanical Engineering, University of New Hampshire, Durham, NH, 03824, USA
[3]UES Inc., 4401 Dayton-Xenia Road, Dayton, OH 45432, USA

Motivation

In order to understand how the processing of AF9628 results in changes in microstructure, it is required to be able to characterize steel microstructures at all stages of processing. This can be difficult for high-temperature steels in the austenite phase, where observing the microstructure directly is difficult. The computational reconstruction of AF9628 is a viable solution to this problem.

Aspects of austenite microstructure have direct impact on final mechanical properties of AF9628 through the control of:

- Prior austenite grain size and morphology
- Austenite texture
- Austenite grain boundaries
- Martensite orientation variant selection

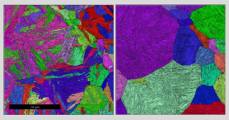

IPF map of a martensitic AF9628 alloy (left). Reconstructed IPF map of austenite structure (right). *(scale bar indicates 100 microns)*

Steel Phase Transformations

The rapid transformation from FCC austenite to BCC/BCT ferrite/martensite:

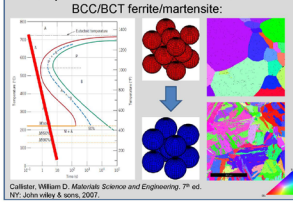

Callister, William D. *Materials Science and Engineering*, 7th ed. NY: John wiley & sons, 2007.

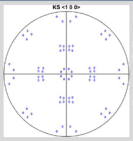

Steels exhibit various orientation relationships between the parent austenite and daughter martensite.

OR	Parallel Plane	Parallel Direction
KS	$\{1\,1\,1\}_\gamma \| \{1\,1\,0\}_\alpha$	$\langle 1\,1\,0\rangle_\gamma \| \langle 1\,1\,1\rangle_\alpha$
NW	$\{1\,1\,1\}_\gamma \| \{1\,1\,0\}_\alpha$	$\langle 1\,1\,2\rangle_\gamma \| \langle 1\,1\,0\rangle_\alpha$
GT	$\{1\,1\,1\}_\gamma$ 1^0 from $\{1\,1\,0\}_\alpha$	$\langle 2\,1\,1\rangle_\gamma$ 2.5^0 from $\langle 1\,1\,0\rangle_\alpha$

Reconstruction Method

For a daughter martensite orientation g^α, the possible parent austenite orientations g_i^γ are given by:

$$g_i^\gamma = T_{OR} \cdot S_i^\alpha \cdot g^\alpha$$

The misorientation between two possible parent orientations is given by:

$$Tr\left(g_i^\gamma g_j^{\gamma^T}\right) = 2\cos(\varepsilon_{ij}) + 1$$

Austenite grouping is achieved by a clustering algorithm that compares the possible parents of individual martensite grains to that of their neighbors.

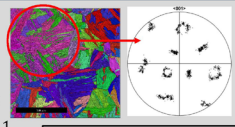

A region of martensite grains that exhibits the KS orientation relationship

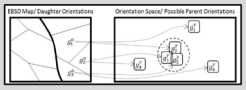

Wrought

Sample 1:

Processing:

- Normalization for 2 hours at 945 °C then air cooled
- Austenitization at 915 °C for an hour then water quenched
- Sub-critical temper at 645 °C then air cooled.

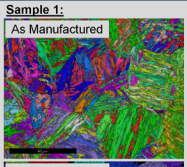

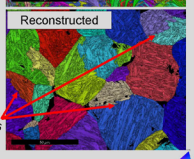

Prior austenite microstructure is primarily equiaxed, possessing some 60° [111] twins. *(Scale bar indicates 50 microns)*

Sample 2:

Processing:

- Normalization for 2 hours at 1050 °C then air cooled
- Austenitization at 825 °C for an hour then water quenched
- Sub-critical temper at 645 °C then air cooled.

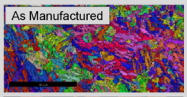

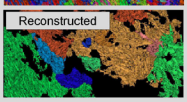

Partial reconstruction shows complex prior austenite boundaries. Lower temperature during second stage of processing likely caused incomplete reaustenitization. (Scale bar indicates 50 microns)

Additively Manufactured

Processing:

- Additively manufactured by laser powder-bed fusion in a PROX 300
- Build direction indicated by arrow

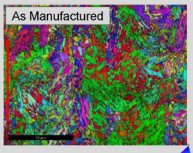

Prior austenite microstructure is primarily columnar, with some larger austenite grains showing mild orientation gradients. *(Scale bar indicates 50 microns)*

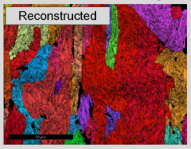

The vertical arrangement of prior austenite boundaries will result in anisotropic properties. The elongated morphology of the parent austenite grains will also affect variant selection of martensite.

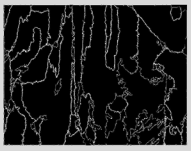

1. Germain, Lionel, et al. "An advanced approach to reconstructing parent orientation maps in the case of approximate orientation relations: Application to steels." *Acta Materialia* 60.11 (2012): 4551-4562.
2. Cluff, S., et al. "Crystallographic reconstruction of parent austenite twin boundaries in a lath martensitic steel." *structure* 1 (2018): 3.
3. Sinha, V., et al. "Correlative microscopy for quantification of prior austenite grain size in AF9628 steel." *Materials Characterization* 159 (2020): 109835.

UNCLASSIFIED

UNCLASSIFIED

The Effects of Surface Functionalization on the Diffusion of Oxygen into the Aluminum Oxide Shell of Aluminum Nanoparticles

Benjamin Evangelisti[1], Chi-Chin Wu[2]

1. Penn State University Department of Chemistry, PhD Candidate
2. Lethality Division, WMRD, CCDC-ARL

Background

Aluminum (Al) powders in the micron-size (mAl) are commonly used as energetic additives due to Al's high heat of combustion (31 kJ/g). Al nanoparticles (nAl) can resolve issues of mAl if their parasitic alumina shell can be mitigated. Preliminary experiments have successfully demonstrated that a carbon coating on surface-modified nAl with a reduced oxide shell thickness leads to enhanced energetic performance.

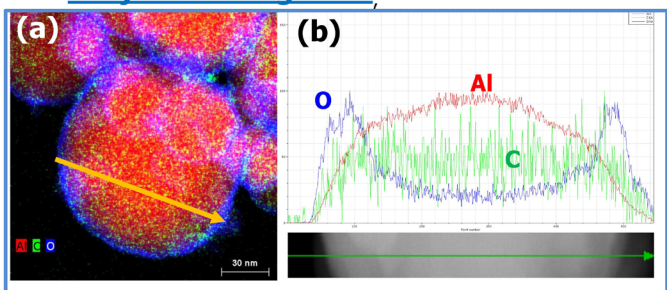

TEM mapping (a) and cross-section intensity profile (b) shows uniform distribution of carbons on the surface of a nAl particle.

Objective

Providing insights of enhanced nAl oxidation through studying the effects of carbon-containing molecules on oxygen (O_2) diffusion into an amorphous alumina slab emulating the nAl oxide shell by using reactive molecular dynamics (MD) simulations.

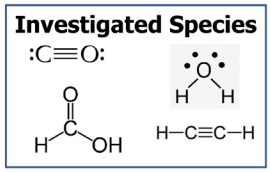

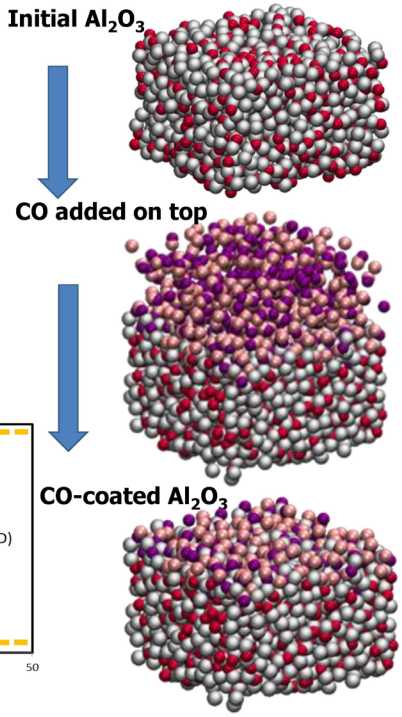

Methodology

An amorphous alumina slab was prepared using COMBAT (a toolkit built in house at ARL[1] to randomly place Al and O atoms and annealed at 2000 K for 100 ps and then cooled to 1000 K over 50 ps in the NPT ensemble. Slab was further cooled to 500 K over 50 ps in the NVT ensemble.

Small molecules such as CO and H_2O were introduced into the vacuum above the alumina surface and reacted at 900 K for 100 ps. Excess molecules were removed to leave a functionalized alumina surface.

The effects of the presence of small molecules and their interactions with the slab on O_2 diffusion was determined by monitoring the unreacted O_2 population during a 200 ps MD simulation.

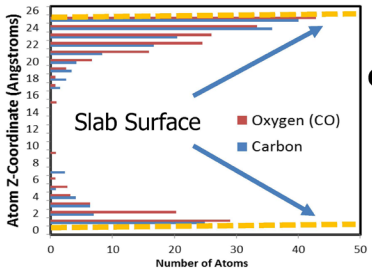

Key Results

The presence of carbon atoms at the alumina surface reduces O_2 diffusion rates by reducing the available sites for entering the bulk alumina phase. More energetically active surface molecules such as acetylene and formic acid display increased O_2 consumption rates by combusting within the alumina layer, potentially destabilizing the alumina further and opening new paths for O_2 diffusion to follow. The results confirms hypothesis drawn from experimental findings.

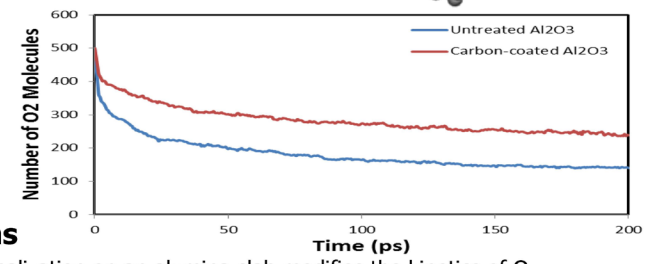

Conclusions

Surface functionalization on an alumina slab modifies the kinetics of O_2 diffusion by reducing O_2 diffusion into the alumina, but increasing the consumption rate of oxygen through combustion.

Acknowledgement

High-Performance Internship (HIP) program
ARL 2020 Summer Student Experience

Reference

1. Anstine D, *et al.* ARL-TR-8914, March 2020

UNCLASSIFIED

QUARTZ PIEZOELECTRIC RESONATORS FOR RF FRONT-END APPLICATIONS UP TO 200 MHz

Mary Beth Galanko, mary.e.galanko.civ@mail.mil
Sarah S. Bedair, Ryan Rudy*, Victor F.-G. Tseng, Jeffrey S. Pulskamp*, Iain Kierzewski

Sensors and Electron Devices Directorate
Energy & Power Division, Power Components Branch (FCDD-RLS-DE)
* Electronics & RF Division, Micro & Nano Materials & Devices Branch (FCDD-RLS-RL)

Objective:

Provide the Army with near-zero-power "wake-up" radios that **monitor contested environments** for RF signals, continuously for a period of months to years, **without the need to replace a battery**.

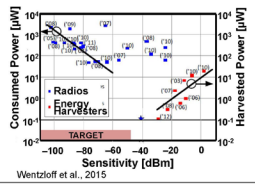

Wentzloff et al., 2015

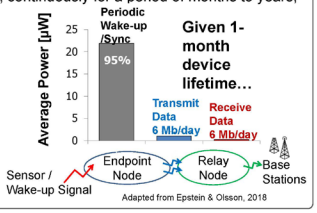

Adapted from Epstein & Olsson, 2018

Performance Survey at 50 MHz

- Voltage gain up to 124 V/V in 2-port coupled resonators
- **Distribution in gain, Q, k^2** validates models of process variation
- In integrated receiver test (transformer + circuit): Demonstrated **sensitivity −79 dBm**

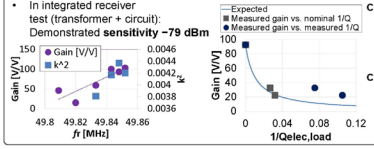

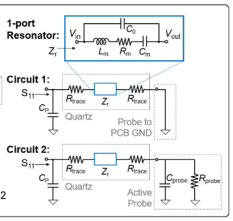

Approach:

Explore quartz as a material for low-power piezoelectric transformers (PTs)

- Investigate achievable **passive voltage gain, quality factor (Q), and matching** to 50 Ω
- Explore advantages of "stacking" multiple quartz substrates
- Integrate with state-of-the-art circuit with power consumption **<10 nW** for sensitivity approaching **−100 dBm**

Traditional receiver (mW): **Typical wake-up receiver (nW):**

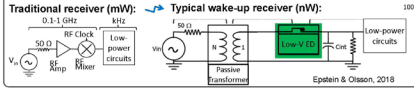

Epstein & Olsson, 2018

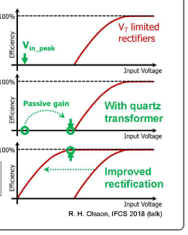

R. H. Olsson, IFCS 2018 (talk)

High-gain Case Study at 75 MHz

- **Gain up to 317 V/V**
  - Limited by testbed Q_{elec}
- ***Q* up to 335,000**
  - Bandwidth ≈ 227 Hz
  - Fits typical wake-up signal bandwidth: 10s-100s of Hz
- **Z_{in} ≈ 100 Ω**
- **Expect sensitivity better than −90 dBm**

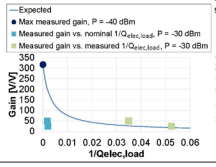

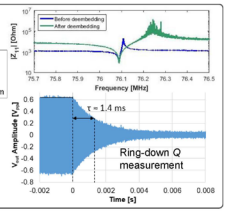

Quartz Resonator Design

Using an established technology in a new way

- Commercially available custom process
- Quartz thickness-shear mode – **high *Q***
  - Create resonant cavity for "trapped-energy mode" standing wave

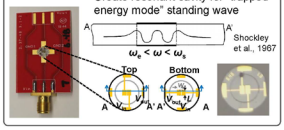

Voltage Gain Testbed

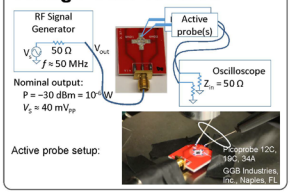

Exploring Higher Frequencies

Technology available up to 200 MHz – how does performance scale?

- Measuring variety of designs to learn:
  - Gain, *Q* vs. resonator geometry
  - Gain, *Q* vs. process variation
- **Current measurements:**

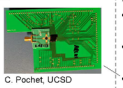

C. Pochet, UCSD

Resonant Frequency	Max Measured Gain	Max Measured *Q* (Ring-down)
93.185 MHz	95	117,000
143.712 MHz	95	133,000
204.175 MHz	300	299,000

Future Work

- Develop **design methodology** to maximize voltage gain
- **Refine testbed** for frequencies >>50 MHz
- Demonstrate **optimized receiver systems** (transformer + circuit) at various frequencies
- Assess technology for **new/broader applications**
  - Spectrum sensing
  - "Internet of Things"

How Should Robots Ask Questions to Maximize Learning? An Empirical Study

Felix Gervits[1], Matthew Marge[1], Genki Kadomatsu[1,2], Gordon Briggs[3], Antonio Roque[2],
Dean Thurston[2], Matthias Scheutz[2]
[1] U.S. Army Research Laboratory, ALC and ARL-NE
[2] Tufts University, Medford, MA
[3] U.S. Naval Research Laboratory, Washington, DC

Overview

- **Present Work:** Empirical study to understand how robots should ask questions to maximize learning when facing uncertainty.
- **Long-Term Goal:** A robot that can automatically generate questions to clarify uncertainty across multiple modalities (e.g. vision, speech, localization).
- **Army Use Case:** More advanced dialogue capabilities for ground robots in scouting, transport, and other applications that involve Soldier-robot interaction.

Methodology

Human participants play the role of a robot on a virtual spacecraft performing a collaborative tool organization task.

-Participant (robot) view.

-Robot can be steered and controlled to pick up and place objects.

Robot communicates with Commander (experimenter) to ask questions via written messages.

-Experimenter view.

-Scripted instructions guide participants through task.

Experimental Stimuli

Task involves identifying tools and opening containers, requiring the learning of novel names and procedures.

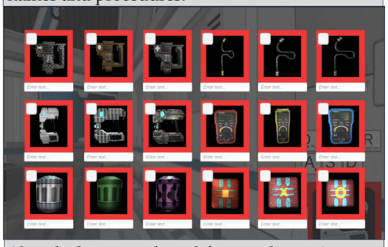

18 tools that vary along 3 feature dimensions.

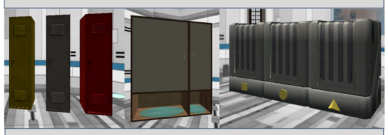

3 types of containers that store the objects.

-Panels that open each of the containers.

-Require learning procedural knowledge to open.

Dialogue Exchange

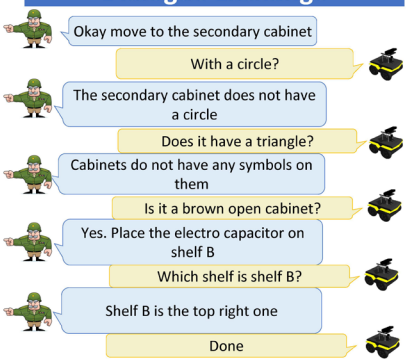

Ongoing/Future Work

- Run study on Amazon Mechanical Turk using interactive networking infrastructure.
- Collect data on *performance*, *time*, *questions*, *workload*, and *situational awareness*.
- Develop scheme of question types from data: Feature clarification - "*You mean the tall one?*" Procedural clarification - "*How do I open it*"? Spatial clarification - "*The one on the left?*"
- Use scheme to train machine learning models for automated question generation.

Bio

Felix Gervits, PhD
Computer Scientist, ARL North-East
gervif@gmail.com

UNCLASSIFIED
Distribution Statement A: Approved for Public Release. Distribution Unlimited.

Detonation of Porous Silicon Nanoenergetics

Philip M. Guerieri[1,*], Wayne A. Churaman[1] (TL), and Brian Fuchs[2]
[1]SEDD, Advanced Electronics Division, Pyro-electronics Team, CCDC Army Research Laboratory (ARL)
[2]Senior Research Scientist for Insensitive Munitions, FCDD-ACD-IM, CCDC Armaments Center (AC)
*FCDD-RLS-EM, philip.m.guerieri.civ@mail.mil

Background

"Metallizing" explosives increases energy density…

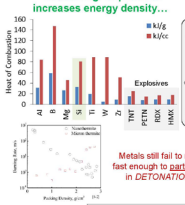

…but requires composite mixtures with slower reaction rates.

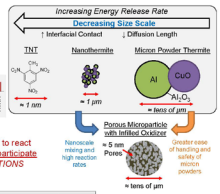

Metals still fail to react fast enough to participate in *DETONATIONS*

Energetic Porous Silicon (PS)

Formed top-down from bulk silicon by HF-etching.

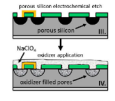

Nitride-masked devices with PS etched into the chip and an ignition wire added.

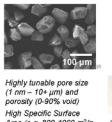

- ✓ *Highly tunable pore size (1 nm – 10+ μm) and porosity (0-90% void)*
- ✓ *High Specific Surface Area (e.g. 800-1000 m^2/g for 2-5nm pores / 70% porous)*

PS Microparticles offer high specific surface area (SSA) of smallest nanothermites with handling ease of microscale powders.

"PSi" 100μm+ ⟷ "Si NPs" <5nm

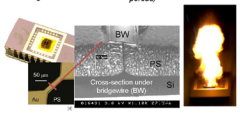

- Rendered energetic by drop casting a solution of solid oxidizer, e.g. Sodium Perchlorate, $NaClO_4$.
- Flame speeds >2 km/s (up to 3.6 km/s with micropatterned surface) surpass the fastest-burning nanothermites.
- Debate in literature over potential of energetic PS to facilitate *detonation*.

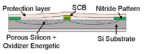

Deflagration

- **SLOWER than speed of sound** in unreacted material (not air).
- Usually <0.5 km/s
- Fast **propagation of a flame** through a flammable material by heat transfer layer by layer.
- Elevated pressure of reaction propagates ahead at speed of sound, forming a **gradual wave** (usually **lower overpressure**, e.g. 50 kPa).
- Possible to initiate with low-energy, e.g. spark or flame.
- Products move away from the propagation reaction.

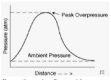

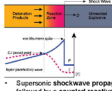

Detonation

- **FASTER than speed of sound** (in unreacted material).
- 1.5 to 9 km/s
- Supersonic **shockwave propagation** immediately followed by a **coupled reactive wave**.
- **Elevated pressure cannot propagate forward** of shock, so onset is sharp and overpressure is usually much higher (e.g. 20 GPa)
- Initiated by a donor shock or transition from accelerating deflagration (DDT).
- Products flow in the direction of propagation within the detonating medium ("particle" velocity).

Objective and Approach

Can energetic porous silicon detonate?

Use CHEETAH 9.0 thermochemical code to model chemistry and apply Chapman-Jouguet (CJ) detonation theory to predict performance. Evaluate by comparison with physical properties and experimental reaction measurements.

In CJ Theory…

- *Fast chemistry*: reactions occur instantaneously at the CJ point just behind the shock front.
- D = U + C (i.e. Detonation or CJ velocity is the sum of particle velocity and sound speed in the products)

CHEETAH calculations…

- Balance chemical potentials across reactions to calculate chemical equilibrium
- Apply CJ assumptions of thermodynamic and chemical equilibrium at the detonation point to predict performance.

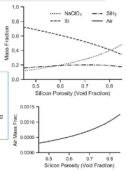

Model formulation compositions based on experimental samples to compare predictions with experimental data. PS porosity considered from 45-85% by volume.

All formulations considered are FUEL-RICH.

69% PS porosity is the experimental average and considered "nominal"

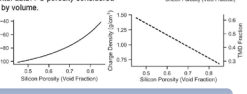

Results

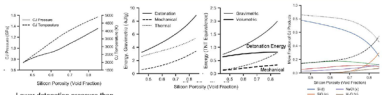

Lower detonation pressure than military explosives (>25 GPa). Exceeds highest overpressure measured from nanothermite (20 MPa (30) by two orders of magnitude.

High Detonation Energy (Thermal + Mechanical) is mostly thermal energy. Atypical for explosives.

More total-energy density than TNT (1-2X) by mass, but lower by volume. Effect of meager charge density.

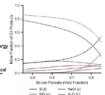

Uniquely low gas production agreeing with low mechanical energy

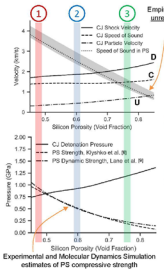

Experimental and Molecular Dynamics Simulation estimates of PS compressive strength

Empirical equation for speed of sound in unreacted PS (shaded uncertainty) [7]

(Recall D = U+C)

Predicts Several Reaction Types:

1. **Low PS Porosity (High density, worst oxygen balance)**
   Unreacted Sound Speed >> Detonation Velocity (Deflagration)
   PS Strength ≥ Detonation Pressure (Deflagration)
   CJ Assumption (Fast Chemistry) is WEAKEST (Overestimation)
   Therefore **detonation is highly unlikely to occur.**
2. **Moderate PS Porosity**
   Unreacted Sound Speed > Detonation Velocity
   PS Strength < Detonation Pressure
   Classical detonation not possible, but a **precompression wave** and PS fracture could support a detonation-like structure.
3. **High PS Porosity (low density, nearest stoichiometric)**
   Unreacted Sound Speed < Detonation Velocity
   PS Strength << Detonation Pressure
   Classical CJ detonation is predicted with rapid catastrophic PS fracture and no sonic precompression wave.

CHEETAH Predicts plausible detonation at high PS porosities

Discussion

Previous works have suggested that flame jumps are a symptom of an underlying sonic compression wave in the PS layer and/or Si substrate.

Comparing CHEETAH predictions with experimental velocities (jump and flame speeds) supports:

- **Precompression waves causing flame jumps at moderate porosities**
- **Detonations possible at moderate and high porosities.**

Fastest energetic PS reactions feature "FLAME JUMPS"

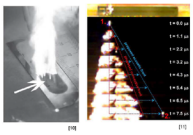

[18] [11]

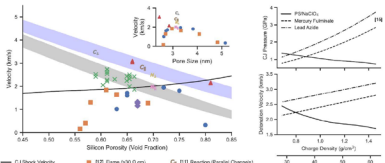

- CHEETAH predictions represent theoretical maximum if FAST CHEMISTRY assumption fits well (poor assumption at lower porosities).
- Several experimental cases approach and match the CHEETAH predictions when pore size is optimal (~3 nm).
- Flame Jump Velocities (Green X) closely match predicted precompression wave velocities (sound speed unreacted at moderate porosity) suggesting the jumps are discrete ignitions caused by a precompression wave.
- Channeled (corrugated superstructure) experiments deviate to high velocities, still plausibly explained by a precompression wave.
- One experimental set deviates high without explaination but has not been replicated since publication.

Nanothermite flame speeds fall rapidly with densification. PS predicted similar but much weaker decrease.

Density remains compared to primary explosives but performance overlaps at low densities.

Conclusions and On-going Work

- CHEETAH thermochemical code predictions of energetic PS detonation performance suggest detonation is possible and occurring is some experimental cases at PS porosities >60%.
- At moderate PS porosities (60-70%), a sonic precompression wave is predicted which can raise reaction rate by inciting discrete downstream ignitions (similar to detonation but more aptly a fast deflagration).
- Supports ongoing work on PS igniters and initiators, 3D printed PS ignition structures, and novel explosive composites for initiation of secondary explosives.

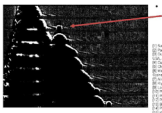

- Preliminary experimental schlieren imaging has observed the predicted sonic precompression wave, possibly causing flame jumps.

This work is currently under review for publication in Combustion and Flame.

[1] Sundaram, D., Yang, V., and Yetter, R.A. (2017) Progress in Energy and Combustion Science 61, pp. 293-365
[2] Fedoroff, B.T., Lynch, J.T., Sharon, J.J., and Henderson, J.E. (2001) Journal of Propulsion and Power, 17(2), pp. 401-410.
[3] Fedoroff, B.T., Lynch, J.T., Ludwig, J.M., Ervin, M.H., and Stanchfield, H.N. (2002) ARL-MR-0514 Picatinny Arsenal, NJ: U.S. Army Research Laboratory, Report No. ARL-MR-0514, 2002.
[4] Dennis, J., and Chudoung, H.S. (2015). 2 Wilkinsburg-Penn Joint Survey, TEC, 2015-007.
[5] Fedoroff, B.T., Lynch, J.T., Ludwig, J.M., Ervin, M.H., and Stanchfield, H.N. (2002) ARL-MR-0514 Picatinny Arsenal, NJ: U.S. Army Research Laboratory, Report No. ARL-MR-0514, 2002.
[6] Klyshko, A.A., Dolbin, A.V., Orlova, V.A., Khmelenko, V.V., Kurnosov, A.V., and Meisner, R.A. (2011) Journal of Applied Physics 110, 063503.
[7] Lane, J.M.D., Grest, G.S., Thompson, A.P., and Ao, T. (2012) Shock Waves 22, pp. 211-221.
[8] Lee, J.W.D., Thompson, A.P., and Aidun, J.B. (2003) MRS Online Proceedings Vol. 759, 9 Empathy, Fl-nda, 6.55.
[9] Fedoroff, Andrew, J., Aydin, T., Snyder, J., Stinson, S.T. (2015) Small 11 (34) 4383-4388.
[10] Fedoroff, A.J., Aydin, T., Snyder, J., Stinson, S.T. (2015) Small 11 (34) 4383-4388. [Contributor not Flame 18] (2) 1431-1439.
[11] Thron, Ann, Jones, C.J., Zunkania, Ind., Gallington, M.E., Ludwig, Eral., Zunkan, J. (2014) Propellants, Explosives, Pyrotechnics v43 (6) 1-9.
[12] Bolen, D.R., Gordon, A.J., Chapman, W.L. (2012) J. Phys. Chem. Solids 73 (11) 1319-1322.
[13] Fedoroff, B.T., Lynch, J.T., Ludwig, J.M., Ervin, M.H., and Stanchfield, H.N. (2002) ARL-MR-0514 Picatinny Arsenal, NJ: U.S. Army Research Laboratory, Report No. ARL-MR-0514, 2002.
[14] Thompson, B., Grest, R., Thompson, B., Sutton, G. (2011) Propellants, Explosives, Pyrotechnics 36 (1) 106-113.

Distribution Statement A: Approved for Public Release. Distribution Unlimited.
UNCLASSIFIED

Communication Constrained Learning for Distributed Hypothesis Testing with Uncertain Models

J. Zachary Hare, Lance Kaplan, Cesar Uribe, Ali Jadbabaie

Objective

Perform distributed classification over a network of agents

Challenges

- Heterogeneous sensing modalities and platforms
- Limited training data for each target class
- Limited communication bandwidth

Relevance

- Human and machine agents collaborating for situational awareness (SA)
- Research Supports Networks/C3I

Problem Formulation

- Agents possess a set of hypotheses $\Theta = \{\theta_1, \dots, \theta_m\}$
- Each hypothesis θ represents a multinomial distribution $P(\cdot\,|\pi_\theta) = \prod_{k=1}^{K} \pi_{k\theta}^{n_k}$
- Each agent i receives a stream of observations $\omega_{i1:t}$ up to time $t \geq 1$, where $\omega_{it} \sim P(\omega_{it}|\pi_{\theta^*})$
- Observations lead to a belief $\mu_{it}(\theta)$ which represent a normalized likelihood ratio
- Utilize Social Learning Theory to aggregate beliefs throughout the network

Current Limitations

- The parameters of the statistical models are known precisely, i.e., π_θ are known exactly
- The agents communication all beliefs at each time step

Solution Approach

1. Model the statistical models with Uncertain Models
2. Select at most one hypothesis to communicate with the largest change in belief
3. Adapt social learning rules to handle dynamic time-varying communications

Uncertain Models

Set of measurements

Set of prior evidence (Training Data)

$$\Lambda_{i\theta}(t) = \frac{\int_{S_\theta} P(\omega_{i1:t}|\pi) f(\pi|r_{i\theta}) d\pi}{\int_{S_\theta} P(\omega_{i1:t}|\pi) f(\pi|r_{i\theta} = \emptyset) d\pi} = \prod_{\tau=1}^{t} \ell_{i\theta}(\omega_{i\tau})$$

Unknown Parameters

$$\ell_{i\theta}(\omega_{i\tau} = k) = \frac{(r_{ik\theta} + n_{it-1} + 1)(t + K - 1)}{(R_{i\theta} + t + K - 1)(n_{it-1} + 1)}$$

Hypothesis Selection

1. Compute the difference
$$\Delta \log(\ell_{i\theta}) = \left|\log(\Lambda_{i\theta}(t)) - \log(\Lambda_{i\theta}(TX_{i\theta}))\right|$$
2. Identify the sets
$$\Theta_{ic} = \{\theta | \Delta \log(\ell_{i\theta}) > \epsilon \text{ and } y_{it}(\theta) > \delta_1\}$$
$$\Theta_{iy} = \{\theta | y_{it}(\theta) > \delta_2\}$$
3. Either select
$$\hat{\theta}_t = argmax_{\theta \in \Theta_{ic}} \Delta \log(\ell_{i\theta}),$$
$$\hat{\theta}_t = argmax_{\theta \in \Theta_{iy}} y_{it}(\theta), or$$
$$\hat{\theta}_t = \emptyset$$

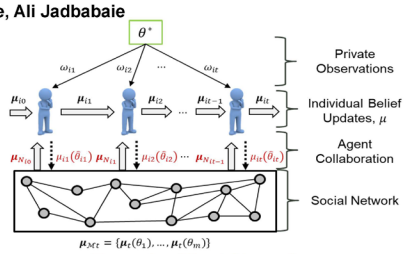

Example of Social Learning

Social Learning Rule

$$\mu_{it+1}(\theta) = \left(\prod_{j \in N_{it}(\theta)} \mu_{jt}(\theta)^{\frac{y_{jt}(\theta)}{d_{jt}(\theta)+1}} \ell_{i\theta}(\omega_{it+1}) \right)^{\frac{1}{y_{ik+1}(\theta)}}$$

Results

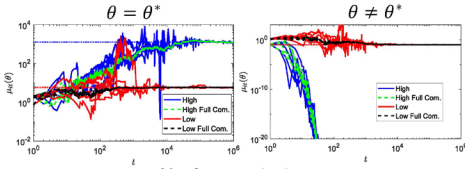

% of transmission

- Low Evidence: 0.15%
- High Evidence: 3.14%

Path Forward

- Quantify the consensus error based on threshold design
- Investigate dynamic thresholds
- Extend hypothesis selection algorithm to include quantized beliefs

Preference Learning for Autonomous Ground Robot Navigation Tasks

Cory Hayes, PhD
cory.j.hayes4.civ@mail.mil
Computational and Information Sciences Directorate

Motivation

- **Overall Goal:** Have robots predict actions of human teammates so they can take a more active role in accomplishing navigation team tasks such as mapping an environment and retrieving information about objects within it.
- **Challenge**: Users interact with technology in different ways, and this depends on a number of factors that make each person unique, along with external factors such as situational context and the desired goal of the interaction.
- **Approach**: We seek to combine human-robot interaction and preference-based reinforcement learning so that an autonomous robot can learn to adapt its behavior based on how the user responds to executed actions.

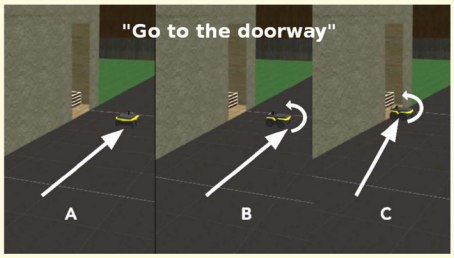

There are many different ways to execute a natural language instruction, with the above examples A-C only being a small subset. Can we learn what a user prefers as a robot builds an interaction history to reduce instruction ambiguity?

Background

- Conducting an ongoing series of natural language dialogue studies [1] where participants give instructions to a remotely located robot in an unfamiliar environment.
- Participants have a limited amount of time to gather certain information about the area via the robot and limited communication channels (no livestream video, instruction delay).
- Formerly a Wizard-of-Oz setup with one wizard acting as Dialogue Manager (DM-wizard) between the participant and the robot, and the other as the robot itself through teleoperation.
- Want to train actual automated DM on naturalistic high-level language instructions, therefore want to **reduce low-level language instructions.** Example: *"Go to the doorway ahead"* vs. *"Move 12 feet forward and turn left 20 degrees"*.
- One cause of low-level language instructions: robot actions that did not meet participant expectations, which leads to corrections through more precise language.
- Solution: learn participant preferences over continued interactions.

Instruction Classes for Navigation Commands

Instruction Type	Example
Approach an entrance	"Go to the doorway"
Enter an unexplored room	"Go into the room in front of you"
Approach another object's vicinity	"Move forward until you reach the crate"
Navigate unexplored areas	"Go to the end of the hallway"
Handle object obstruction	"Move around the cone"
Follow direction only instruction	"Go to the left"
Follow direction + orientation instruction	"Head three feet north"
Fulfill an impractical task	"Move forward 8 feet" (robot <8 ft from wall)

- In previous work [2] towards addressing the problem, we pinpointed eight instruction classes from the dialogue corpus that spanned the types of commands that participants gave to the robot.

User-Specific Autonomous Navigation

- **Goal:** Allow for personalized robot navigation behaviors that meet user expectations by modifying a copy of the generalized navigation model per user and refining it over multiple interactions.
- Participants give instructions through speech recognizer to autonomous robot that can perform standard SLAM-based navigation, collect user dialogue over interactions to pinpoint rejections of robot actions through clarifications/corrections and acceptances.
- Data collection methods: Robot simulation software (Gazebo) with virtual environments, audio of participants, multiple interaction sessions per participant with TBD exploration tasks to accurately gauge navigation improvement over time.
- **Method:** Preference-Based Reinforcement Learning to modify navigation models between user sessions based on user and environmental rewards. This method is similar to standard reinforcement learning except the model learns preferences between trajectories (state-action sequences) instead of relying on arbitrarily set rewards, allowing for more flexibility for reward design and user expertise.
- **Intended Outcome**: Navigation models that vary per participant and lead to shorter navigation task completion times with fewer corrections for robot behavior.

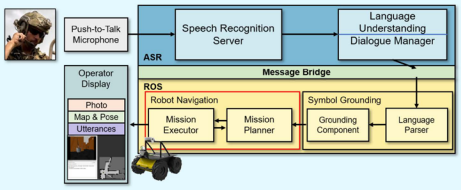

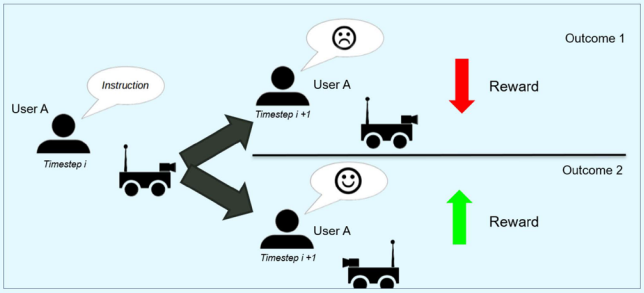

Above: Simplified illustration of the planned capability of the preference-learning navigation algorithm. "User A" gives a verbal instruction to a robot who then executes the behavior, and in return the user either has a negative (top right) or positive (bottom right) response to the robot's actions to be used as reward signals.

Left: End-to-end pipeline for the components that enable the above functionality. A participant speaks into a microphone and their input is converted to text by our automated speech recognition (ASR) software. The text is then forwarded over a message bridge to our Robot Operating System (ROS) software that provides all robot functionality and simulation. The section outlined in red is where the proposed work falls into the pipeline.

Challenges / Open Questions

- Incorporating verbal user feedback as a part of the reward function for the RL phase will require careful manual annotation of user responses to accurately identify acceptance of robot actions and corrections/clarifications, and this can lead to ambiguous input that may need to be resolved by sentiment analysis techniques.
- What navigation features will be sufficient to reliably parameterize user-preferred navigation to use as part of the environment reward?
- What is the stopping criteria for the number of trials required in the model training phase to show that the robot has adapted to a user's navigation preferences?
- High-level commands such as "Go to the doorway" will require the robot to either have existing knowledge of the environment or be able to determine landmarks on the fly. Which approach is ideal for our scenario?

Acknowledgements

This research was sponsored by the Army Research Laboratory and was accomplished under Cooperative Agreement Number W911NF-16-2-0117. The views and conclusions contained in this document are those of the authors and should not be interpreted as representing the official policies, either expressed or implied, of the Army Research Laboratory or the U.S. Government. The U.S. Government is authorized to reproduce and distribute reprints for Government purposes notwithstanding any copyright notation herein.

1. M. Marge, C. Bonial, A. Foots, C.J. Hayes, C. Henry, K. Pollard, R. Artstein, C. Voss, D. Traum. "Exploring Variation of Natural Human Commands to a Robot In a Collaborative Navigation Task". *In Proc. of the 1st Workshop on Language Grounding for Robots*, pp. 58-66, 2017.
2. P. Moolchandani, C.J. Hayes, M. Marge. "Evaluating Robot Behavior in Response to Natural Language". *Companion of the 2018 ACM/IEEE International Conference on Human-Robot Interaction*, pp. 197-198, 2018.

Annealing behavior of point defect complexes in irradiated 4H-SiC

Robin Karhu, Daniel Habersat, Donald Fahey, Albert Burk, Brenda VanMil

Abstract

Point defects in wide bandgap semiconductors have in recent years attracted interest for their spin coherence properties [1]. The most well studied example is substitutional Nitrogen with a nearest neighbor vacancy (NV) complex in diamond. Similar properties can be found in point defects in other wide bandgap semiconductors such as Silicon Carbide (SiC). Benefits of using Silicon Carbide as opposed to diamond is the much more mature manufacturing process, such as commercially available substrates and homoepitaxial layers up to 150 mm in diameter and electronic devices such as MOSFETs. Using the point defects is SiC has the benefit of merging existing processing capabilities with emerging quantum information technology.

The defects of interest in SiC are the Silicon vacancy (V_{Si}) and the divacancy ($V_{Si}V_C$) [1-3]. These defects are created by irradiating SiC samples with electrons followed by annealing at different temperatures. At the moment there is a lack of understanding in the creation process of these defects. In this work the defect evolution in SiC homoepitaxial layers irradiated with electrons are tracked using Deep level transient spectroscopy (DLTS) and photoluminescence (PL). The study will compare DLTS and PL spectra as a function of temperature and electron irradiation dosage.

Typical results of electron irradiation

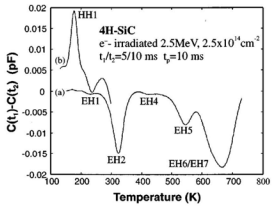

FIG. 1. DLTS spectrum observed in 4*H* SiC irradiated by 2.5 MeV electrons with a dose of 2.5×10^{14} cm^{-2} with t_1/t_2 = 5/10 ms and a pulse width of 10 ms (a) with a reverse bias of −9 V and a pulse height of 9 V and (b) with a reverse bias of −9 V and a pulse height of 12.5 V.

[4]

Preliminary data

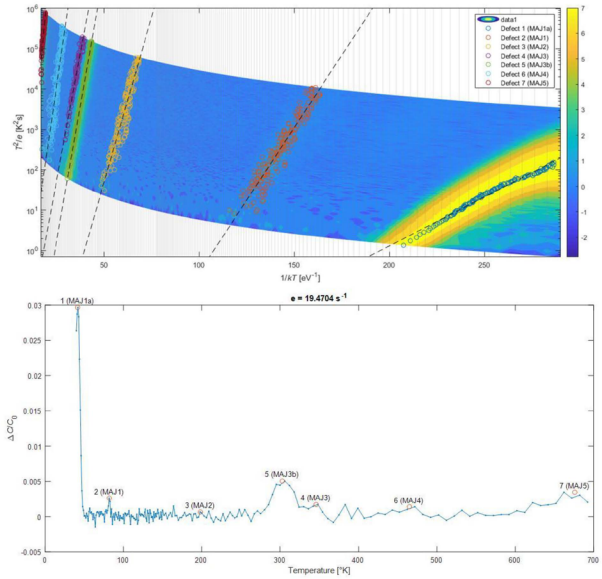

Sample A: As grown 4H-SiC homoepitaxial layer
Sample B: Oxidized 4H-SiC homoepitaxial layer
Sample C: Electron irradiated (2 MeV) 4H-SiC homoepitaxial layer

	MAJ2			MAJ3b			MAJ4			MAJ5		
	Capture cross section [cm^{-2}]	Trap concentration [cm^{-3}]	Energy level [eV]	Capture cross section [cm^{-2}]	Trap concentration [cm^{-3}]	Energy level [eV]	Capture cross section [cm^{-2}]	Trap concentration [cm^{-3}]	Energy level [eV]	Capture cross section [cm^{-2}]	Trap concentration [cm^{-3}]	Energy level [eV]
Sample A				2.8E-16	8.7E11	0.59	1.2E-17	3.6E11	0.80	1.0E-18	4.5E11	1.15
Sample B				9.3E-16	8.8E11	0.60	1.4E-17	3.6E11	0.81			
Sample C	1.0E-15	3.7E11	0.38	1.5E-15	1.7E12	0.61	3.2E-18	3.4E11	0.74	3.2E-18	1.6E12	1.19

To do

Investigate if the transformations of the point defects and point defect complexes can be observed with DLTS and PL. Also try and correlate the less studied DLTS peaks to defects in 4H-SiC.

Referencees

1. Weber, J.R., et al., *Quantum computing with defects.* Proc Natl Acad Sci U S A, 2010. **107**(19): p. 8513-8.
2. Son, N.T., et al., *Divacancy in 4H-SiC.* Phys Rev Lett, 2006. **96**(5): p. 055501.
3. Janzén, E., et al., *The silicon vacancy in SiC.* Physica B: Condensed Matter, 2009. **404**(22): p. 4354-4358
4. Hemmingsson, C., et al., *Deep level defects in electron-irradiated 4H SiC epitaxial layers.* Journal of Applied Physics, 1997. **81**(9): p. 6155-6159.
5. Rauls, E., et al., *Metastability of the Neutral Silicon Vacancy in 4H-SiC.* physica status solidi (b), 2000. **217**(2): p. r1-r3.

UNCLASSIFIED

Stimuli-Responsive Phase-Change Materials for Adaptive Imaging Systems & Microactuation

Cory R. Knick[1], Adam A. Wilson[2], Gabriel L. Smith[2], Daniel Jean[2]
US Army C5ISR Center, Night Vision and Electronic Sensors Directorate (NVESD), Ft. Belvoir, VA 22060
U.S. Army Research Laboratory, Sensors and Electron Devices Directorate (SEDD), Adelphi, MD 20783

PURPOSE

Leading the development of next-generation adaptive imaging systems based on stimuli-responsive phase change materials

BACKGROUND

Stimuli-responsive phase change materials are classified by their ability to adapt or reconfigure in response to external stimuli (temperature, light, pH, magnetic/electric fields, etc.) and will enable the next generation of adaptive imaging systems.

Phase-change materials can serve as the foundational building block of microactuators which can be used to dynamically reconfigure optical elements to enable reconfigurable imagers with multi-functionality.

Application spaces for these materials encompasses variable light transmission, MEMS micromirrors, laser beam steering, adaptive optics, spatial light modulators (SLM), micro-robotics, and actuation.

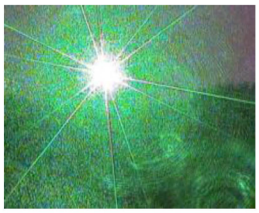

Sensor looking at bright light source

Reconfigurable imager (micromirror, spatial light modulator, dynamic filter, etc.)

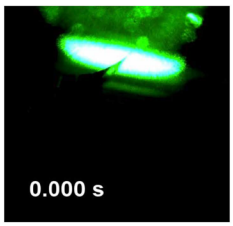

Reversible laser actuation of Shape Memory MEMS

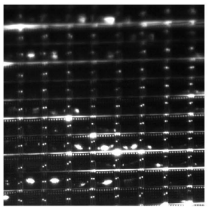

Laser actuation of micromirror array

LWIR IMAGING SYSTEM WITH LENS AND FPA

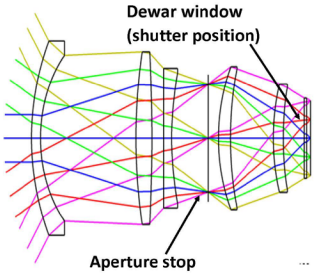

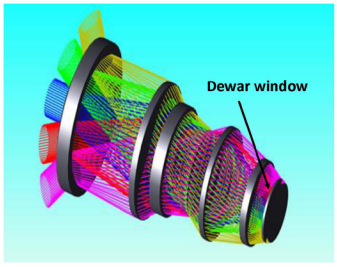

MECHANICAL AND OPTICAL PROPERTIES

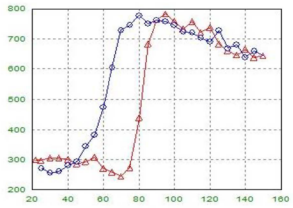

Stress change in thin film VO_2 vs. temperature

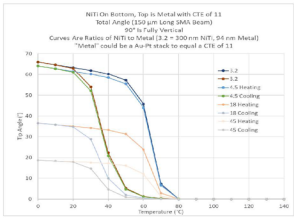

Modeled actuator performance based on NiTi SMA bi-layer actuator

ELECTRICAL ACTUATION OF SMA MEMS

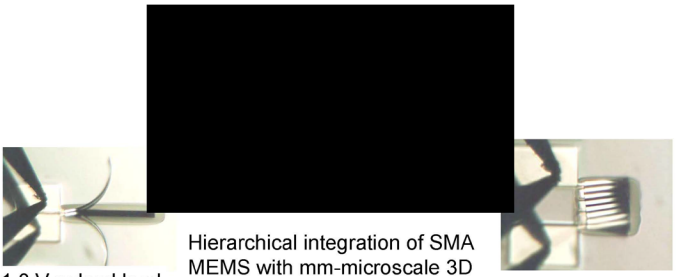

1.0 V pulsed load

Hierarchical integration of SMA MEMS with mm-microscale 3D printing for microrobotic actuation (CMU collaboration)

Force multiplication

PROCEDURE

- Sputter deposition of NiTi SMA and VO_2
- MEMS micromirror/static filter fabrication in ARL's SEMASC
- Modeling actuation performance
- Characterization of materials and devices across the phase-transition: TEM, SEM, FDTR, TDTR, FTIR

REFERENCES

https://iopscience.iop.org/article/10.1088/1361-6439/ab1633
https://www.sciencedirect.com/science/article/abs/pii/S0924424718320089
https://www.sciencedirect.com/science/article/abs/pii/S0924424719305400
https://www.peosoldier.army.mil/programs/ivas/
https://www.army.mil/article/226591/u_s_army_gvsc_ngcv_cft_demonstrate_phase_1_concepts

CONCLUSIONS & FUTURE WORK

- Optimize materials & micromirror performance.
- Tune stress and material property changes.
- System integration and testing
- Refine phase-change properties through rigorous investigation of processing conditions
- Substrate / epitaxial growth
- Novel compositions
- Pursue technology transition opportunities: Next Gen Combat Vehicle (NGCV), Integrated Visual Augmentation System (IVAS)

UNCLASSIFIED Cory R. Knick, Ph.D. cory.r.knick.civ@mail.mil 937-564-7321

Compositionally-Mixed Interfaces and Thermal Boundary Conductance at Pt-silicide/Si Interfaces

Dr. LeighAnn Larkin[1,2], Dr. Pamela Norris[1]
1 University of Virginia, Mechanical Engineering
2 Army Research Lab, SEDD

Thermal Boundary Conductance, h_{BD}

h_{BD} manifests as a finite and discontinuous drop in temperature at an interface.

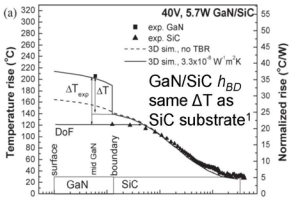

In densely packed devices, h_{BD} can cause self-heating.

When conduction is dominated by phonons, the available phonon density of states at the interface limits h_{BD}.

Enhancing PDOS Overlap

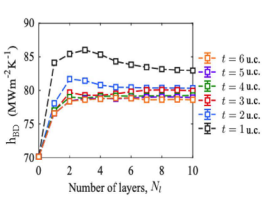

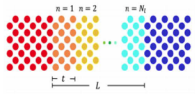

Computational results suggest composition-grading the interface could enhance h_{BD} at vibrationally-mismatched interfaces[2]

Objective: Create a compositionally-graded interface and measure its effect on h_{BD}

Time Domain Thermoreflectance, TDTR

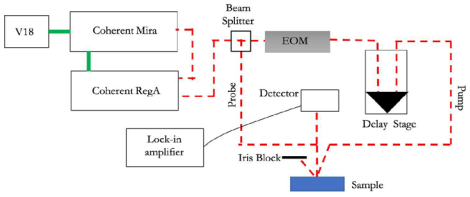

Pump beam deposits a Gaussian-shaped heat-source and probe beam monitors changes in the surface reflectivity, correlated to surface temperature.
The pump and probe are temporally delayed to generate a cooling profile and measure unknown thermal properties, such as h_{BD}.

PtSi/Si Growth

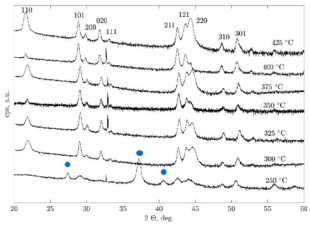

XRD spectra of co-sputtered and annealed samples
Miller indices of PtSi phase labeled, blue dots = possible β-Pt_2Si

Pt and Si were co-sputtered onto a Si substrate and annealed to promote diffusion at interface

PtSi/Si Interface

Interfacial thickness estimated as region encompassing 90% to 10% of average film

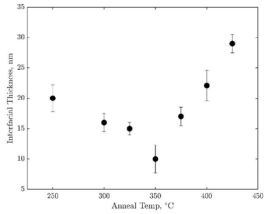

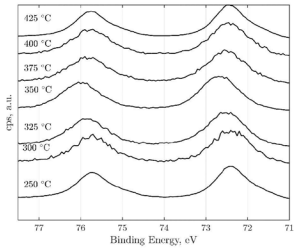

Pt4f XPS peaks at half-way through interfacial region

XPS results demonstrated interfacial region composed of PtSi and atomic Si phase for all samples

Results: h_{BD}

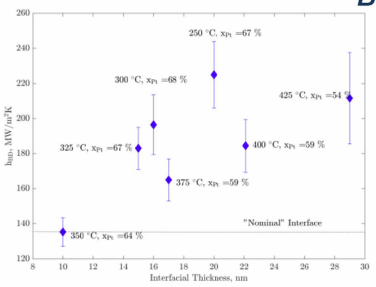

h_{BD} of PtSi/Si increased with increasing interfacial thickness

- h_{BD} linearly related to the interfacial thickness
- Faster transitions in composition resulted in higher h_{BD}
- Linear relation suggests compositional-grading could enhance phonon re-thermalization contributing to h_{BD}.

[1] A. Sarua, et al. *IEEE Transactions on Electron Devices* (2007).
[2] R. Rastgar, et al., *Nanoscale* (2019).

CONCEPT OF SELF-PHASED ELEMENTS IN REFLECTARRAY AND TRANSMITARRAY ANTENNA

Quang Nguyen and Amir I. Zaghloul
CCDC Army Research Laboratory, SEDD, Adelphi, MD, 20783
quang.m.nguyen7.ctr@mail.mil, amir.i.zaghloul.civ@mail.mil

Objectives

- Propose a concept of self-phased elements used in the reflectarray and transmitarray antenna
- Self-phasing results from dynamically controlling the effective permittivity of the antenna substrate
- Explore tunable dielectric substrates by applying a DC bias to the material

Current State-of-the-Art

- Needs to create the phase shifts between antenna elements in the array to steer the main beam to desired directions
- This can be done by using feed network, incorporated with phase shifters
- The cost of phase shifters is up to half of the total cost of the entire scanning phased array system

Self-Phased Elements in Reflectarray

- Present an example of reflective beam steering design composes of 8x8 circular inter-digitated self-phased (CID-SP) places on top of dielectric layers which uses a constituent material

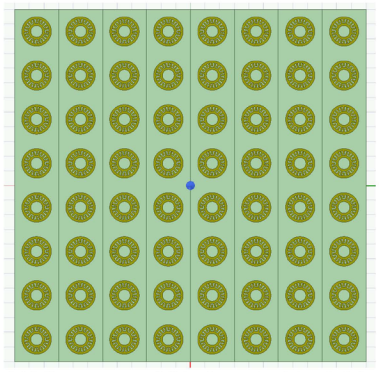

The proposed MTS composes of 8-by-8 circular inter-digitated self-phased (CID-SP) cells. Each column has an independently tunable BST substrate permittivity ε_r. By changing the by a bias voltage applied to the BST, the desired reflection (Rx) phase can be achieved. The dimensions of the 8-by-8 are $L_x = L_y = 48$ mm. The height of the R-MTS is $h = 1$ mm, which is $\lambda_0/24$ at the operating frequency of $f_0 = 12.8$ GHz

- Perform HFSS finite R-MTS array simulations to scan the reflected beam to θ_r = +26 deg for incident plane waves with horizontal, vertical, and slant polarizations.

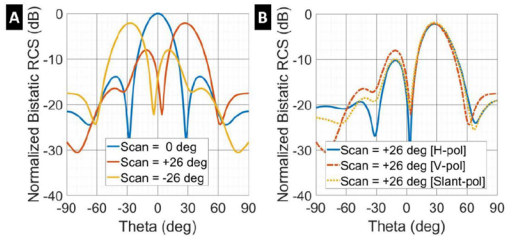

Self-Phased Elements in Transmitarray

- Present an example of phased array systems composes of self-phased elements placed on top of conventional probe-fed patch antennas

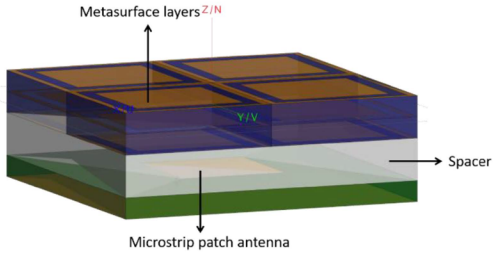

Geometry of proposed single-element phased array system

- Perform simulation on 20 degrees beam steering capability of three-element phased array at 9.1 GHz

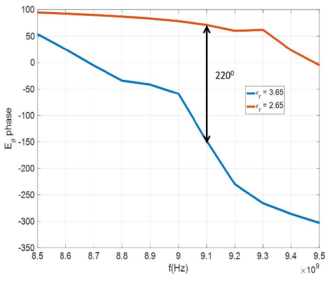

Simulated radiation pattern of the proposed three-element phased array system

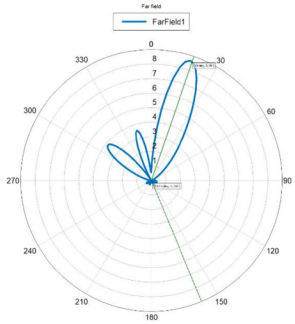

Simulated radiation pattern of the proposed three-element phased array system

UNCLASSIFIED

Photoelectrochemistry of III-V Epitaxial Layers and Nanowires for Solar Energy Conversion

Vijay S. Parameshwaran
U.S. Army Research Laboratory, Sensors and Electron Devices Directorate, Adelphi, MD 20783

Introduction & Motivation

- **Solar-driven chemical reactions:**
  - Water to hydrogen gas
    $$H_2O + h\nu \rightarrow \frac{1}{2}O_2 + H_2$$
  - Carbon dioxide to high-order fuels
    $$CO_2 + 2H_2O + h\nu \rightarrow \frac{3}{2}O_2 + CH_3OH$$

Onsite fuel generation for army deployment

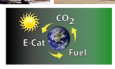

- **Electrical junction studies of nanomaterials**
  - Liquid Schottky barrier at interface
  - Direct analog to solar fuels reactions
  - Testbed for materials, electronic, and photonic properties with scaling

Oxidation/Reduction

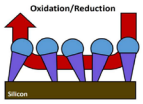

- **Why III-V Semiconductors?**
  - Direct bandgap tunability for light absorption and photovoltage
  - High crystallinity for charge transport and low SRH recombination
  - Electrolyte chemical stability with engineering passivation layers

InGaP and GaP Epitaxial Layers

- *Use MOCVD to grow epitaxial undoped InGaP on p⁺ GaAs and GaP on p⁺ Si, with high crystal quality and a large depletion region*

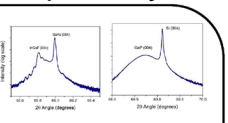

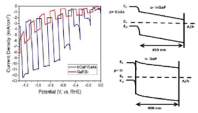

- *Both sets of junctions drive non-aqueous $MV^{+\bullet}$ reduction and hydrogen evolution*
- *EIS study confirms extended depletion junction design as reflected in band diagrams*

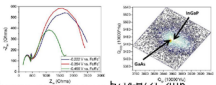

- *Thicker films do not correlate to increased performance, tied to dislocation defects (InGaP) and junction decoupling (GaP)*

J. Electrochem. Soc. 163 (7), pg. H474-H721, 2016

Structured GaN

- **Control of film, microwires, and nanowires**
- *Change film (and junction) with source material amount and spacing using reactive vapor phase transport*

Thick Films | Mixed Films/Wires | Nanowires w/ Islands

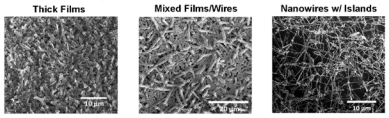

- *Films are polycrystalline, nanowires and islands are single crystal*

•Photoanode configuration on p⁺ silicon

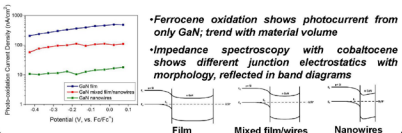

- *•Ferrocene oxidation shows photocurrent from only GaN; trend with material volume*
- *•Impedance spectroscopy with cobaltocene shows different junction electrostatics with morphology, reflected in band diagrams*

J. Electrochem. Soc. 163 (10), pg. H958-H963, 2016

InP and GaP Nanowire Cathode

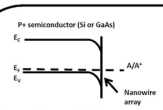

GaP on Si | GaP on GaAs | InP on Si | InP on GaAs

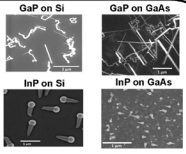

- *Grow InP and GaP nanowires on p⁺ Si and p⁺ GaAs, respectively, to form a cathode*

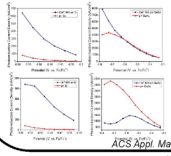

- *GaP nanowires show an increased photocurrent for both Si and GaAs*
- *InP nanowires show an increased photocurrent for Si, but not for GaAs, because of InGaAs interlayer formed*
- *Nanowires on GaAs show fourfold <111> orthogonality, epitaxial-like matching to substrate*

ACS Appl. Mater. Interfaces, 8 (33), pg. 21454-21464, 2016

InN Nanowires

- **•Control of wire shape through VLS growth process**

Indium Catalyzed | Gold Catalyzed

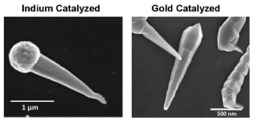

- *In-catalyzed with thermal gradient: "ice cream cone" structure*
- *Au-catalyzed at low temperature: wide-base faceted cone*
- *Both nanowire forms are wurtzite hexagonal binary InN, and single crystal*

•Photoanode configuration on p⁺ silicon, cobaltocene

- *•Cobaltocene oxidation under solar flux shows photovoltage, but capacitance shows highly charged interface consistent with InN surface accumulation*

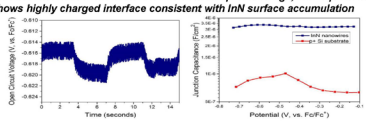

ACS Appl. Mater. Interfaces, 8 (33), pg. 21454-21464, 2016

Fe:NiO_x OER Catalyst on Nanowires

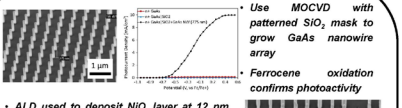

- *Use MOCVD with patterned SiO_2 mask to grow GaAs nanowire array*
- *Ferrocene oxidation confirms photoactivity*
- *ALD used to deposit NiO_x layer at 12 nm and 36 nm, with treatment in iron solution to enhance activity*
- *Through process, nanowires were not structurally degraded*

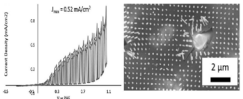

- *OER driven by both thickness films, 12nm film electrode failed from pinhole defects*

J. Electron. Mater., 47 (2), pg. 932-937, 2018

UNCLASSIFIED

TECHNOLOGY DRIVEN. WARFIGHTER FOCUSED.

UNCLASSIFIED

Porous Silicon Inks for Safely 3D Printed Explosive Structures

Katherine M. Price*, Philip M. Guerieri, Matthew Ervin, and Wayne A. Churaman (TL)

SEDD, Advanced Electronics Division, Pyro-electronics Team

CCDC Army Research Laboratory (ARL)

Summary

Energetic porous silicon (PS) microparticles with nanoscale porosity and high internal surface area (~800 m^2/g) offer the high heterogenous reaction rates associated with nanoscale fuel/oxidizer mixing in a safer and more easily handled microparticle architecture. In this work, ink formulations, processing methods, and printing procedures are under development for direct write of polymer-bound porous silicon microparticle beds. Post-print, these structures can be rendered explosive by application of a solid oxidizer solution into the internal nanostructures. Binder selection is critical to facilitate this post-print activation. Compared to alternative energetic inks with all reactive ingredients included, printing only the fuel improves safety and cost efficiency especially for manufacture of microscale ignition structures with sensitivities comparable to primary explosives. Initial flame-speed measurements exceeding 700 km/s demonstrate the effective emulation of on-chip energetic PS reactivity with 3D printed and post-print activated structures.

Background: Igniter Technologies

Conventional Electric Match (aka Fuze Head, Hot Wire Igniter)

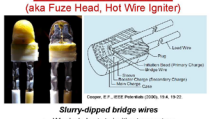

Slurry-dipped bridge wires

- Wire joule-heats to ignition temperature
- Large volume requirements and low precision

Semiconductor Bridge (SCB)

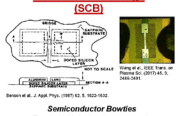

Semiconductor Bowties

- Electrical initiation by plasma expansion
- HIGH POWER requirements

Nanothermites

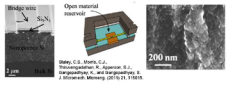

e.g. nAl/Bi_2O_3 Nanothermite in reservoir on SCB

- Predominantly Aluminum with metal oxides (Boron in development)
- Can require hazardous expensive nanoenergetic powder handling
- Low reaction rates compared to explosives (improving with on-going research), especially when densified.
- Native oxide passivation layers limit energy density

Reactive Foils (Nanolaminates)

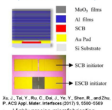

- Highly precise microfabrication
- Moderate to high energy release rates and energy density
- Expensive

Energetic Porous Silicon (On-Chip)

Strong primary energetic system is made from the Si chip itself under SCB

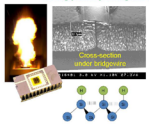

Pores filled with solid oxidizer (e.g. drop-cast $NaClO_4$ solution in methanol)

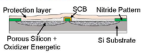

$$(1-n)Si + nSiH_2 + \frac{2+n}{4}NaClO_4 \rightarrow SiO_2 + NaCl + nH_2O$$

- Critically high internal surface area (800-1000 m^2/g)
- High precision microfabrication, direct Si chip integrations
- Flame speeds: 0.01-2 km/s; up to 3.6 km/s with superstructure
- Ignite via heat, spark, or friction
- Low power and energy ignition threshold
- Native hydrogen surface termination is reactive

Objective

- 3D print energetic PS, more substrate/geometry agnostic, to enable rapid prototyping of conformal ignition structures
- Polymer binder for mechanical stability compatible with post-print incorporation of oxidizer (i.e. printed inert and post-activated)
- Minimize adverse binder/printing effects on ignition and reactivity

Fabrication/Approach

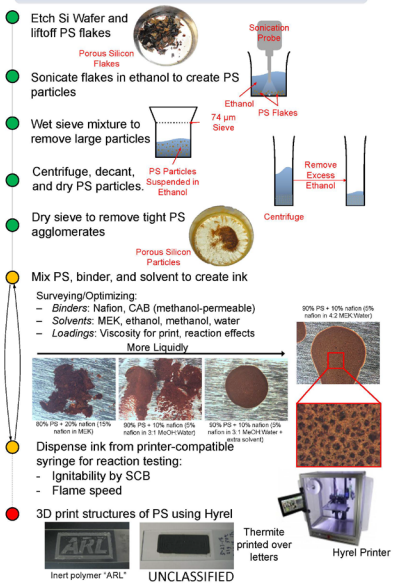

Results

SCB/Bridgewire Ignition: ***Successful***

80 wt% PS + 20 wt% Nafion polymer (MEK solvent)

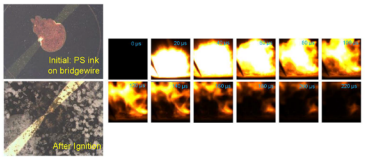

Reaction Flame Speed: ***576 m/s***

90 wt% PS + 10 wt% Nafion (3:1 vol MeOH:Water cosolvent)

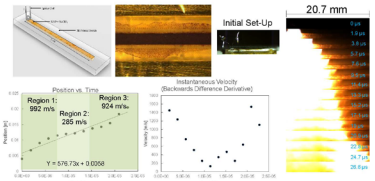

Conclusions and On-going Work

- ✓ **Proven concept: direct write of Nafion polymer-bound PS microparticle beds with oxidizer solution permeation post-print to render explosive**
- ✓ **Bridgewire ignitable and flame speed >700 m/s**
- ❑ **High vapor pressures of Nafion solvents complicate processing and printing – continuing binder and solvent survey**

Other on-going work and paths forward:

- Use Hyrel 3D printer to print on various substrates to evaluate effects of reaction heat and pressure.
- Embed ignition methods within printed structure.
- Introduce bomb calorimetry to measure heat of combustion of prints.
- Evaluate effect of recipe changes on measured flame speeds.
- Procuring rheometer to characterize ink rheology for printing.
- 3D print superstructures seeking novel effects on reaction and ignitability, including graded microparticle size with multiple-ink prints.
- Prototype novel igniter devices with low volume and flexible geometry.

*FCDD-RLS-EM, katherine.m.price11.ctr@mail.mil

Synthesis and Characterization of Novel, Broadband Nonlinear-Absorbing Chromophores

Objective

Our objective is to develop new, panchromatic reverse saturable absorption (RSA) materials that exhibit broadband ground- and excited-state absorption features.

Think Transitions® Lenses Technology

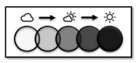

RSA occurs when the excited-state of a molecule absorbs light more strongly than its ground state at the specific wavelength of interest.[1] This property makes RSA agents great candidates for applications like sensor and eye protection from high intensity light sources.

Development Loop

The *ARL RSA Material Development Loop* is the high-throughput methodology through which we design, synthesize, characterize, and test potential RSA chromophores.

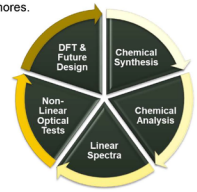

1. Chemical Synthesis: Design and synthesize target molecules; **2. Chemical Analysis:** Confirm structural identity and purity; **3. Linear Spectra:** Obtain ground state absorption spectra and investigate linear photophysical properties; **4. Non-Linear Optical Tests:** Obtain excited state absorption spectra and evaluate RSA performance; **5. DFT and Future Design:** Use computational chemistry to model materials and use results to guide future targets.

Implementation of the ARL RSA Development Loop

1. Chemical Synthesis:

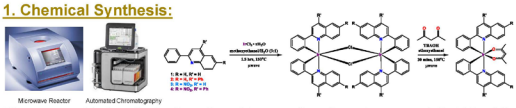

Microwave-assisted synthesis allows for quick generation of novel organometallic iridium(III) complexes[2-4] such as the Ir(III) bisphenylquinoline acac. Purification is achieved by automated chromatography which reduces the required time and solvent. This high throughput methodology can produce a series of novel RSA agents in days whereas conventional means could take weeks.

2. Chemical Analysis:

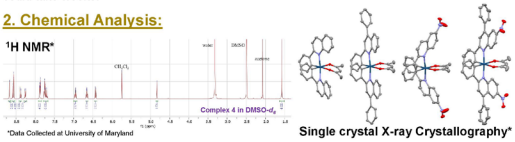

The complexes were characterized by ^{1}H NMR and single crystal x-ray crystallography confirming the structure to be the typical isomer for [Ir(C^N)$_2$(acac)] of *cis-C,C/trans-N,N* geometry with typical bond lengths and are highly pure.

3. Linear Spectra:

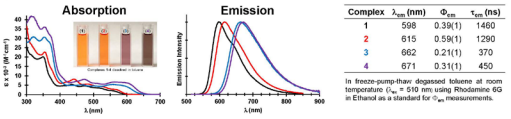

Complex	λ_{em} (nm)	Φ_{em}	τ_{em} (ns)
1	598	0.39(1)	1460
2	615	0.59(1)	1290
3	662	0.21(1)	370
4	671	0.31(1)	450

In freeze-pump-thaw degassed toluene at room temperature (λ_{ex} = 510 nm using Rhodamine 6G in Ethanol as a standard for Φ_{em} measurements.

All samples exhibit characteristic absorption bands: ligand-centered (LC) π-π* transitions (300-400 nm) and metal-to-ligand charge transfer (MLCT) d-π* transitions (400-700 nm).[5] The addition of the phenyl and/or nitro group result in broader absorption of visible light (+ ~50 nm for nitro group). The additional phenyl group results in higher molar absorptivity values (+ ~1,000 $M^{-1}cm^{-1}$). When irradiated with 510 nm light, the complexes are emissive with λ_{max} ranging from 598 nm to 671 nm and with emission lifetimes ranging from 370 ns to 1460 ns. The additional phenyl group increases the emission quantum yield, whereas the addition of the nitro group decreases emission quantum yield.

4. Non-Linear Optical Tests:

Transient Absorption

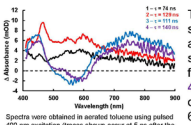

Spectra were obtained in aerated toluene using pulsed 400 nm excitation (traces shown occur at 5 ns after the pulse).

Transient absorption data shows that complexes **1** and **2** exhibit broad excited state absorption (positive features), whereas, **3** and **4** do not (negative features or bleaches from ~500 to 600 nm).

ps Z-Scan

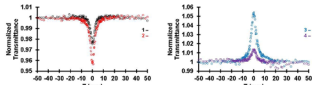

Open-aperture picosecond Z-scan experiments of these complexes in aerated toluene (λ_{ex} = 532 nm 110 nJ, 30 ps FWHM)[6]

1 and **2** exhibit RSA (decrease in transmittance) when irradiated with 532 nm, whereas complexes **3** and **4** show saturable absorption (SA, an increase in transmittance) as predicted from transient absorption data.

5. DFT and Future design:

Density functional theory (DFT) gives information on where electron density is located in the ground and excited state and can be used to predict ground state and excited state absorption.

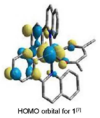
HOMO orbital for 1[7]

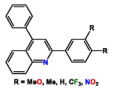

Future efforts will focus on modification of the cyclometalating ring with variety functional groups. Due to the negative impact on the excited state absorption, the nitro group will be eliminated while maintaining the 4-phenyl group due to its beneficial impacts.

References: [1] W. M. Shensky, *et al., Appl. Opt.* 2017, **56**, B179. [2] A. K. Nedeltchev, *et. al., Tetrahedron*, 2010, **66**, 9319. [3] G. C. Muscia., *et al.,Bioorg. Med. Chem. Lett.*, 2014, **24**, 1545. [4] T. M. Monos, *et. al., J. Org. Chem.*, 2016, **81**, 6988. [5] Y. You, W. Nam, *Chem. Soc. Rev.* 2012, **41**, 7061. [6] M. Sheik-Bahae, *et al., IEEE J. Quantum Electron*, 1990, **26**, 760. [7] L. Chen, *et. al., ChemElectroChem*, 2017, **4**, 1797.

Acknowledgments: The authors would like to thank Dr. Fu Chem and Dr. Yinde Wang of the UMD Analytical NMR Service Center for their assistance with NMR measurements.

UNCLASSIFIED // APPROVED FOR PUBLIC RELEASE

POINT OF CONTACT:
Thomas N. Rohrabaugh, Jr., Ph.D.
Thomas.n.rohrabaugh.civ@mail.mil
301.394.1720

Co-Authors: Ryan M. O'Donnell, Trenton R. Ensley, Peter Y. Zavalij (UMD), Michael J. Ferry, and William M Shensky III

High Speed Detection Characterization of Event-based Sensors

Jonah Sengupta, Benjamin Linne, Aaron Bard

U.S.ARMY · DEVCOM ARMY RESEARCH LABORATORY · JOHNS HOPKINS WHITING SCHOOL of ENGINEERING

Abstract

Event-based sensors have demonstrated latencies on the scale of 1-10 microseconds making the technology an energy-efficient, lightweight option for real-time, high speed object detection and tracking. Research has been conducted to characterize the sensor's abilities to detect high-speed objects in a controlled-environment to establish performance upper limits and induce what on-chip channels and physical mechanisms act as bottlenecks. A configurable LED strip with user interface was designed and implemented to extract this detection cutoff in a lab-controlled environment. A user-interface was embedded into the LED strip to allow for customization of the simulated projectile's "velocity". Using a custom signal processing algorithm, the location of the projectile tip was extracted. **By tracking the number of average tip positions over the range of recorded shot velocities, linear extrapolation shows the absolute limit of the event-based sensor to be 1450 m/s.**

Objectives

- Create a controlled experimental set-up to systematically capture optical projectiles with the event-based sensor
- Use recordings to gather a first estimate of a detection velocity limit for a specific event-based sensor

Materials and Methods

Configurable LED strip

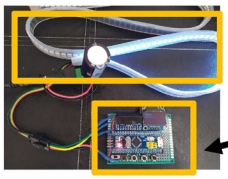

Adafruit Dotstar LED strip: 144 LEDs with local brightness and color control via in-pixel microcontrollers

LED Controller Protoboard: controls operation of strip, contains - LCD display, BluePill microcontroller, and push buttons to control projectile velocity

Event-Based Sensor

DAVIS 346 and Tele Lens

Specification	Value
Spatial Resolution	346x240
Temporal Resolution	1us
Max Throughput	12 million events per second
Dynamic Range	120 dB
Dimensions	40x60x25mm
Weight	100g
Power consumption	0.9W

Sensor Specifications

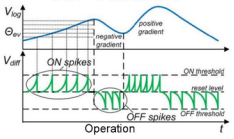

- Inspire by the mammalian retina, event-based sensors ***asynchronously*** respond to ***changes in intensity*** rather than encode absolute values in frames
- Positive changes produce **ON** events and negative changes produce **OFF** events

Experimental Set-up

- Dimensions of lower panel are 11.5" x 18.5"
- Sensor is 18" above the LED strip.
- LED projectile propagates from left to right across the sensor FOV and is acquired via NVS connected via USB 3.0 to laptop

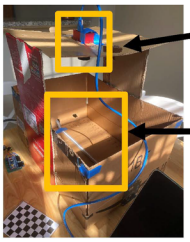

Results

Algorithm

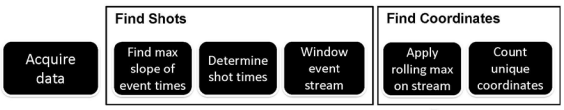

Shot Detections

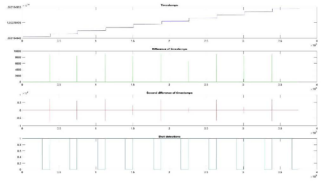

Use event timestamps to find shots using maximum of derivative with respect to index

Address Rolling Max

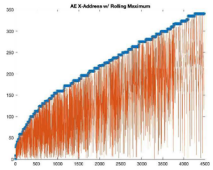

Find maximum X-address across FOV via iterative algorithm

Detections

Velocity (m/s)	Optical Flow (pix/us)	Detected X-Addrs. (# of pix)
50	0.042	131.3
100	0.084	113.6
250	0.210	85
350	0.294	79.5
500	0.420	77.0
750	0.630	54.7
1000	0.840	47.3

Results from 7 recorded shots: optical flow was calculated using calibration parameters, detections were averaged across 3 shots/recording

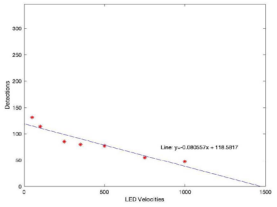

Recorded velocities vs. Detections: linear interpolation is overlaid over 7 datapoints. Equation of line-of-best-fit inline

Conclusions

- Via linear interpolation of current detections, the detection velocity limit of the DAVIS346 is 1450 m/s
- Given certain operation conditions, event-based sensors seem to offer a lightweight, efficient solution to detect high-speed threats

Future Steps

- **Modify Event-Based Sensor:** use another event-based sensor to understand relationship of resolution with respect to detection limit. Reconfigure event-based sensor parameters for low-latency acquisition
- **Data collection**: collect more velocities – past 1000 m/s, populate current intervals

Acknowledgements

- This work and effort has been sponsored by the DoD-funded SMART Fellowship
- The authors would like to thank the support staff at iniVation for important advice regarding event-based sensor calibration

Known & Unknown Risk Identification and Data Encoding to Improve C2 Decision-Making in Multi-Domain Environment

Relevant to IOBT CRA Research Area / Task: Research Area 1, Task 1.1 and Research Area 3, Task 3.3

Objectives

1. Uncertainty mitigation by focusing on small data challenges in order to improve C2 decision-making in Multi-Domain Environments (MDE).
   - Improve decision-making confidence by compensating in model's low performance with *known* & *unknown* knowledge.
2. Increase situational awareness by encoding data in military operations when machine learning models tend to overfit on a small dataset.
   - To investigate methods to maintain data privacy during information transmission over an IoT network.

Approach

1. Encode information (image) into audio signals.

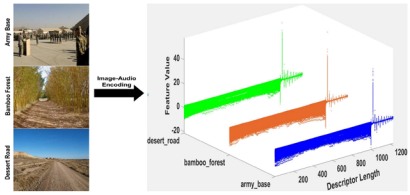

2. Quantify uncertainties by identifying the regions of *known* & *unknown* risks.

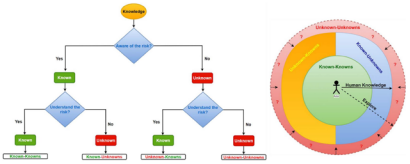

Figure: *A visual representation of our proposed approach to illustrate the premises of known and unknown pairs. The frontier of human knowledge become ambiguous and chaotic as we move away from the center outside the **green** region and step into the other colored regions. The '**?**' represents region that needs to be explored. Dotted circumference of **red** region indicates unboundedness of this region due to the lack of any knowledge about this region and its existence. Dotted arrows pointing inwards indicate that the goal should be to converge this red region to any possible **yellow**, **blue** or **green** region. In that order, ideally every encompassing region should be converged to a region it encompasses.*

Results

Table: *Comparison of models' performances. We used **128 GB RAM** CPU and **NVIDIA Quadro P3200 6144MB.- Memory Type: GDDR5 (Samsung)** GPU.*

Model	Data	Platform	Model Run Time (Hours-Minutes-Seconds)
Transfer Learning	Image	CPU	0 : 14 : 05
DNN	Audio	GPU	0 : 01 : 17

Image Data (Before Encoding) | **Audio Data (After Encoding)**

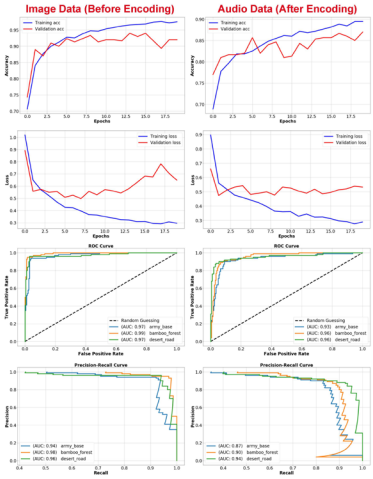

Figure: *Comparative analysis with Transfer Learning on image data and DNN on audio data shows that we were able to retain most of the information in image-audio encoding. Some patterns are lost in encoding process due to data nuances as shown in another figure. This pattern loss can be compensated with proposed known & unknown approach in order to improve confidence in decision-making.*

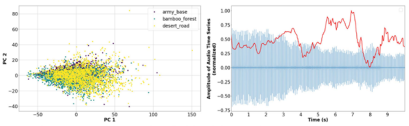

Figure: *Challenges of data nuances in audio data obtained after image-audio encoding.*

Conclusions

1. We proposed a paradigm involving pairs of *known* & *unknown* knowledge which can provide a better understanding of uncertainties (risks) arising from unforeseen events and ease of their assessment.
2. This approach can increase the confidence level in decision-making process when model performance is limited due to small data size.
3. We formulated our experiments with challenges similar to the U.S. Army's IoBT CRA project with three classes, categorized as; red (enemy), gray (neutral), blue (friend) assets.

Path Forward

1. We will investigate data regularities and how the data patterns are impacted by image-audio approach.
2. Investigate methods to relay information over an unreliable network in order to sustain an uninterrupted line of communication for mission success and C2 decision-making.
3. We will generate scenarios realistic to the actual problem.

Publications

[1] P.K. Sharma, "Heterogeneous and Noisy Short Signal Camouflage to Image & Audio for C2 Decision Making in Multi-Domain Environment", in the *Transactions on Mass-Data Analysis of Images and Signals. (2020).*

[2] P. K. Sharma and A. Raglin, "Image-Audio Encoding to Improve C2 Decision-Making in Multi-Domain Environment", in *25th International Command & Control Research and Technology Symposium (ICCRTS 2020).*

[3] P. K. Sharma and A. Raglin, "Image-Audio Encoding for Information Camouflage and Improving Malware Image Pattern Analysis," in *17th IEEE International Conference on Machine Learning and Applications* (ICMLA 2018).

U.S. ARMY RESEARCH, DEVELOPMENT AND ENGINEERING COMMAND — RESEARCH LABORATORY

POINT OF CONTACT:

Piyush Sharma, Ph.D.
piyush.k.sharma.civ@mail.mil
301-394-5609

UNCLASSIFIED// APPROVED FOR PUBLIC RELEASE

Solid State Power Emulator to Evaluate (SSPE) ½ H-Bridge Module

Richard Thomas, US Army Research Lab

Purpose of the SSPE

From an electrical perspective as solid state devices are developed by the level and pattern of the doping used to create the them, circuit testing is needed to confirm simulated behavior as a result of the changes that it was made with. This is also needed as advancements are made for device mechanics and temperature management. Many times device failure destroys the device and its surrounding support due to the high power needed to test it. The SSPE was developed to subject the device under test (DUT) to the maximum switching and on-state operation power while it only requires 10% of what is usually needed to drive the test. The reduction of system power improves safety, reduces size and allows less damage to the DUT if failure occurs.

Process of the SSPE

The SSPE provides both a high voltage and a low voltage power source. They can be operated separately or together. This allows for different type of circuit operation if a device would be subject to simple high voltage switching or soft current switching or full switching. The figures below show the switching of 500V and 42A at 50% of 10kHz. Normally system power needed for this test is 10.5kW however to provide the full switching the SSPE needs only 1.1kW.

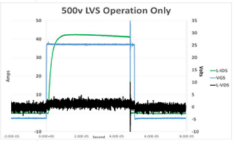

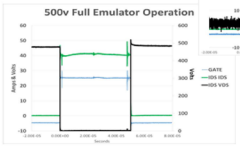

½ H-Bridge Testing with SSPE

The combination of mechanical and thermal structures for mosfets known as the "Power Tower" needed testing of its benefits when devices are in the ½ H-Bridge configuration. This would normally need a maximum power of 24kW for operation at 600V, 50A at 10kHz. The SSPE was modified to support this type of circuitry only requiring ~5kW.

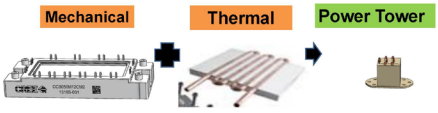

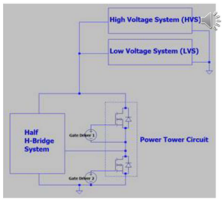

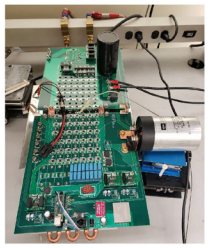

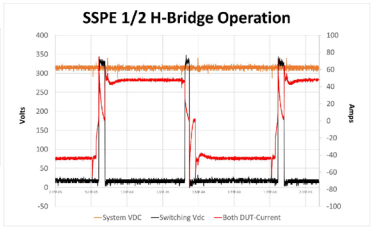

Progression of The SSPE

The development of low inductance motors with values in the single digit micro Henry's has given a challenge to current driving methods with that use pwm and require an external inductance. With this external inductance speed of the motor is limited to its value and power efficiency is reduced. An analog method is being investigated to replace the normal pwn method and would not need an external inductance and will not be limited in operation speeds. The modified analog SSPE provides a waveform that is similar to a device operating the analog motor driver. The benefit of the SSPE testing is that the motor is not in jeopardy while the device is tested. This will only require 1/6 of the normal operation power.

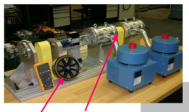

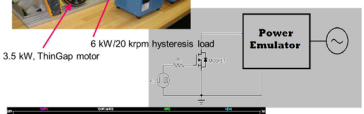

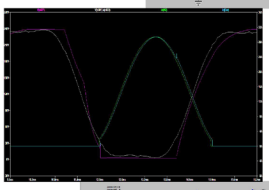

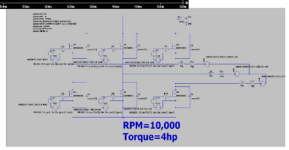

α-Sn Magnetotransport Devices

Authors: **Owen Vail**, Patrick Folkes, Patrick Taylor, George de Coster

Low-Power Topological Electronics

Opportunity: Reducing power consumption at the tactical edge provides an opportunity for extended mission duration while meeting requirements for game changing computational technologies in mobile and autonomous platforms: Artificial Intelligence, Machine Learning, Advanced Sensor Processing. *Topological electronics* enable ultra-low power high-speed devices for next gen. information processing

α-Sn Devices

Approach: As a *single-element topological material*, diamond cubic α-Sn provides a platform for a wide array of devices through its topologically protected spin-momentum locked surface state. Coupling this material to magnetic materials or signals will provide drastic power and space reductions for the future of device technologies.

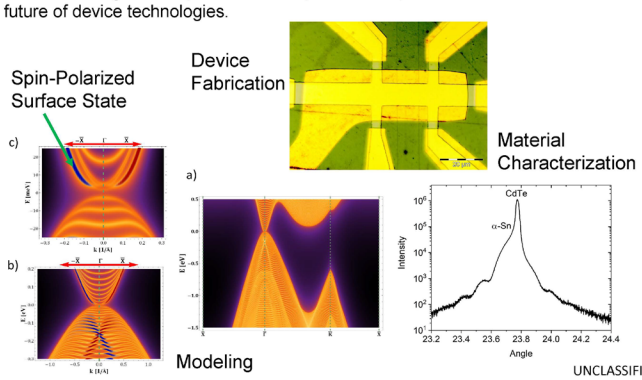

Magnetotransport and Gating

Method: As Gated magnetotransport devices provide intricate details of material behavior and characteristics, providing a direct measurement of the electronic response as well as carrier densities and mobilities involved.

Temperature Dependence of Electrostatic Gating

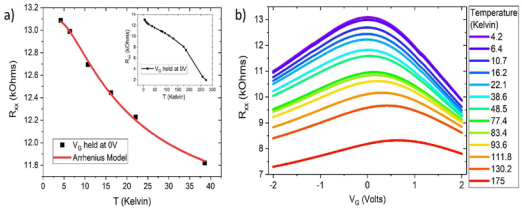

Gated Magnetotransport as a Tool for Electronic Characterization

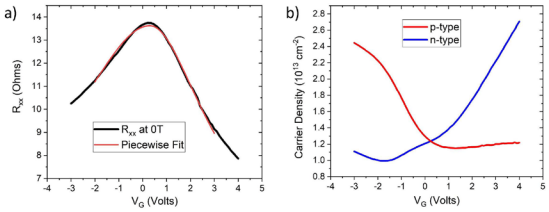

Toward Optical Interfaces for Quantum Networks:

Characterization of Optical Coupling between SNAP Microresonators and Tapered Optical Fibers

Dashiell L. P. Vitullo, Quantum Networking Team, TNAB, CISD
Email: Dashiell.L.Vitullo.civ@mail.mil

Motivation

Quantum systems have capabilities that classical systems fundamentally cannot match. Entanglement is the fragile resource that enables these capabilities. Optical microresonator systems are promising as optical interfaces capable of handling entanglement, connecting nodes to channels, and routing entangled photons in quantum networks.

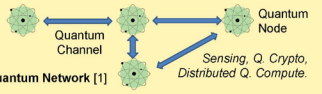

Quantum Network [1]

Example Quantum Network Elements:

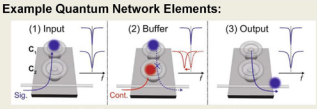

All-Optical Buffering (photon storage) [2]

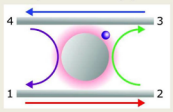

Single-atom-controlled Circulator [3]

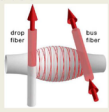

All-optical Switching (photon routing) [4]

SNAP Microresonators

Sufrace nanoscale axial photonics (SNAP)

- ✓ Microresonators on fiber/capillary surfaces
- ✓ Ultrahigh intrinsic Q ≈ 10^8
- ✓ Subangstrom fabrication precision [5]

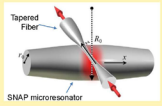

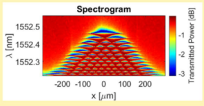

Approach

Quantum-compatible microresonator systems require:

- ☑Slow tunability [6]
- ☑Coupling characterization [7]
- ☐Loss minimization
- ☐Fast all-optical coupling control

Status

Developed and demonstrated robust coupling characterization methodology using the Local Coupling Approach [7].

Transmitted Power — Green's functions (All-mode distribution)

$$P(\lambda,x,z)=\left|S_0(z)-\frac{i\,|C(z)|^2\,G(\lambda,x,x)}{1+D(z)G(\lambda,x,x)}\right|^2$$

$|S_0|$: Nonresonant transmission

$|\Psi(x)|^2$: Single mode distribution

$\mathrm{Re}(D)|\Psi(x)|^2$ Resonance Shift

$\mathrm{Im}(D)|\Psi(x)|^2$ Broadening/ resonant loss

Not shown: $\arg(S_0)$: Fano Resonance shape

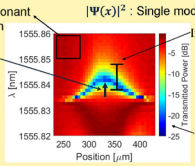

$|C|^2|\Psi(x)|^2$ Depth

$$D_{ex}(z)=\mathrm{Im}[D(z)]-|C(z)|^2\frac{1-\mathrm{Re}[S_0(z)]}{1-|S_0|^2}>0$$

Broadening beyond energy conservation limit

$$B_{crit}(z)=\frac{|S_0(z)|^2\mathrm{Im}[D(z)]}{\mathrm{Re}[S_0(z)]}$$

Undercoupled: $|C|^2>B_{crit}$ Critically Coupled: $|C|^2=B_{crit}$ Over-coupled: $|C|^2<B_{crit}$

Critical Coupling Bound

Characterization successful in all coupling regimes

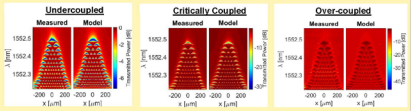

Coupling Parameters

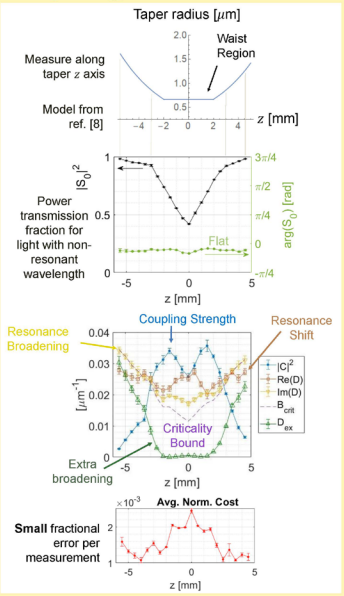

References

[1] H. J. Kimble, Nature **453**, 1023 (2008).
[2] W. Yoshiki et al., Sci. Rep. **7**, 10688 (2017).
[3] M. Scheucher et al., Science **354**, 1577 (2016).
[4] M. Pollinger and A. Rauschenbeutel, Opt. Express **18**, 17764 (2010).
[5] N. A. Toropov and M. Sumetsky, Opt. Lett. 41, 2278 (2016).
[6] D. L. P. Vitullo et al., Opt. Lett. **43**, 4316 (2018).
[7] D. L. P. Vitullo, S. Zaki, D. E. Jones, M. Sumetsky, and M. Brodsky, Opt. Express **28**, 25908 (2020).
[8] L. Ding et al., Appl. Opt. 49, 2441 (2010).

Phonon transparency at high interface density of nanolaminate thin films

Our goal is to pursue ways to **tailor thermal conductance** in electronics packaging:

- Higher conductance → improved SWaP in high power systems
- Lower conductance → improved sensitivity in temperature detection

Interface thermal conductance (G_{int})= relatively unexplored channel for tailorability of thermal properties

$$G_{int} = \frac{1}{4}\sum \int_0^{\omega_{A,j}^{v}} \underbrace{D_{A,j}(\omega)}_{\text{Phonon density of states}} \underbrace{\frac{\partial n(\omega,T)}{\partial T}}_{\text{Change in phonon modes vs temperature}} \underbrace{\hbar\omega v_{A,j}}_{\text{Phonon group velocity}} \underbrace{\alpha_{A\to B,j}(\omega)}_{\text{Phonon transmission coefficient}} d\omega$$

Integrating over vibration frequencies

Diffuse mismatch model (DMM)

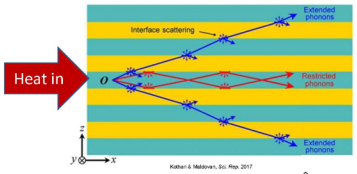

Assuming diffusive scattering at **every** interface.

$$\alpha_{A\to B,DMM} = \frac{\sum_j D_{B,j} v_{B,j}}{\sum_j D_{A,j} v_{A,j} + \sum_j D_{B,j} v_{B,j}}$$

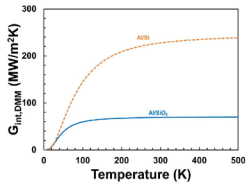

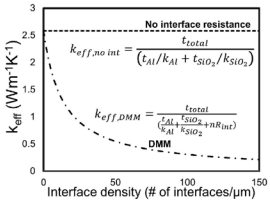

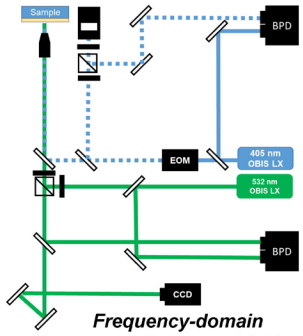

Frequency-domain thermoreflectance (FDTR)

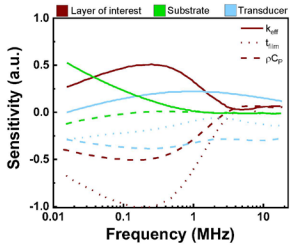

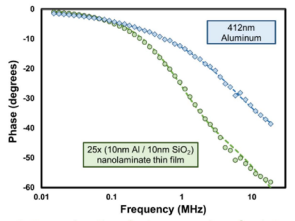

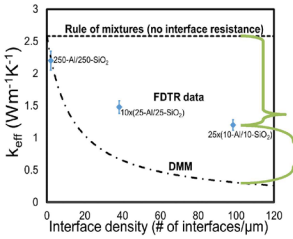

>2.5x reduction in k_{eff} vs rule of mixtures

DMM under-predicts k_{eff} by >3x

Using simple, widely available materials, we show:

- Lower conductance by >2.5x at ~100 interfaces/μm
- Higher conductance than predicted by DMM

Future work:

- Change density, stress, surface roughness by material deposition and preparation parameters to determine effect on interface thermal conductance

Adam A. Wilson[1], Darin J. Sharar[1], Ronald Warzoha[2], Andrew Smith[2]
[1]*Sensors and Electron Devices Directorate, CCDC Army Research Laboratory*
[2]*Department of Mechanical Engineering, US Naval Academy*

UNCLASSIFIED

Antibody-Recruiting Protein-Catalyzed Capture Agents as a Therapeutic for COVID19

Alexander Winton[1], Matthew Coppock[1], Sanchao Liu[1], Bert T. Lai[2], Anders Eliasen[2], Matthew N. Idso[3], James P. Hopkins Jr.[3], Sanchao Liu[1], Jessica Yee[3], Sunga Hong[3], Rachel Calder[3], Katrine Museth[2], Fred Mast[4], Heather Agnew[2], Michael Klimas[2] and James R. Heath[3]

(1) CCDC Army Research Laboratory, Adelphi, MD, (2) Indi Molecular, Inc., Culver City, CA, (3) Institute for Systems Biology, Seattle, WA, (4) Center for Global Infectious Disease Research, Seattle Children's Research Institute, Seattle, WA

COVID-19, a coronavirus which emerged in late 2019, has resulted in an ongoing global pandemic with more than 22 million confirmed cases and over 775,000 deaths as of August, 2020. While remdesivir, dexmethosone and convalescent plasma have exhibited some success in treating hospitalized patients, their use is limited to severe cases and there is currently no FDA approved therapeutic. Protein Catalyzed Capture (PCC) agent research is currently pursued at ARL as an alternative to state-of-the-art antibody recognition elements for sensor applications, as these agents address gaps in discovery time, batch-to-batch variation, and exhibit cost effective and scalable manufacturability. The current Covid-19 project demonstrates the untapped versatility of PCC agents, where discovered recognition elements may be employed beyond detection applications, as a therapeutic to treat an emerging disease threat. By making modular modifications to PCC sensing elements (addition of a hapten moiety) a therapeutic may be rapidly developed (in tandem with a sensing element), capable of recruiting a person's endogenous antibodies to aid in clearing foreign pathogens. Ultimately, this research will enable the Future Army to rapidly and effectively respond to emerging biological threats by providing sensing and therapeutic capabilities.

SARS-CoV-2 Epitope Discovery for Therapeutic Screening

SARS-COV-2 is a single stranded RNA virus that encodes 4 structural proteins – S, E, M, N. The Spike protein is responsible for binding host cell receptor and membrane fusion and is the predominant antigen for neutralizing antibodies. Bioinformatics and Molecular modeling were employed to identify promising epitopes for therapeutic targeting.

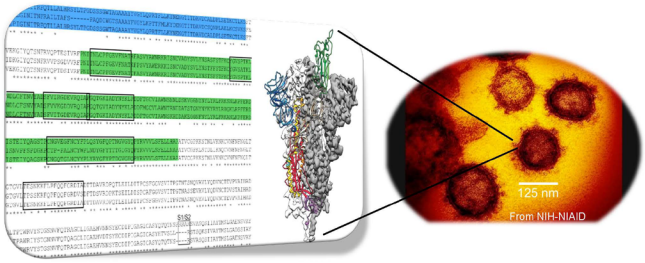

Epitope	# of Hits
1	33
2	26
3	8
4	21
5	17
6/7	22
Total	**127**

Identification of PCC Leads by Library Screening

Epitope targets are chemically synthesized and screened against a PCC library composed of unnatural amino acids. The PCC technology utilizes an *in situ*, un-catalyzed "click" reaction to identify entropically favored PCC lead compounds exhibiting nanomolar target affinity. This project has utilized a teaming approach, leveraging capabilities from Army, Industry and Academia.

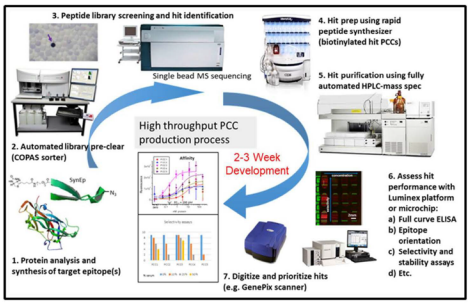

PCC Lead Validation, Down-selection, and Preliminary Antibody Recruitment

Identified PCC lead affinities are validated using a High-throughput Luminex assay. A majority of PCCs exhibit on-bead affinities in the low nanomolar region. Specificity screening against various other proteins such as ACE2, SARS-Spike, and the RBD domain were performed to down-select from initial candidates and subsequent EC_{50} values under various buffer conditions were determined. Preliminary ELISA screening depicted PCC leads capable of antibody recruitment!

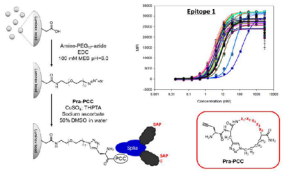

Epitope	PCC	EC_{50} in T20 (nM)	EC_{50} Glycine Washed (nM)	EC_{50} in 1% Serum (nM)	EC_{50} in 5% Serum (nM)
1	nyme	5	13.9	163	353
1	nnpdh	3.8	10.6	155	303
1	tgam	3.1	16.0	173	426
2	nylvv	5.7	41.8	317	459
2	tnehs	5	15.4	175	323
2	vwyge	5.2	8.3	116	278
3	wisdk	27.9	348	340	527
3	kdlvw	24.7	483	307	428
3	nifda	5.7	10.2	156	325
4	dpafa	5.8	4.0	110	277
4	ergnv	8.2	5.4	124	297
5	aalwd	18.7	16.9	154	312
5	sattl	15.7	4.8	115	297

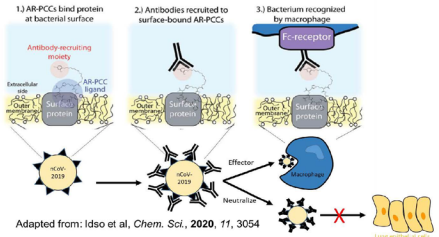

Adapted from: Idso et al, *Chem. Sci.*, **2020**, *11*, 3054

PCC Solution Affinity/Recruiting Assay Development and Testing

Further development of Solution based assays for PCC binding have been developed. An adapted Luminex Screening method covalently attaches target proteins of interest to magnetic beads and PCCs that are free in solution are screened for affinity. Single point assays were initially utilized to identify promising PCC leads and subsequent K_d values were obtained under various screening conditions (Optimization is on-going). Surface Plasmon Resonance has also been utilized in conjunction with the modified Luminex assay and has demonstrated consistent affinity trends.

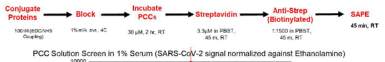

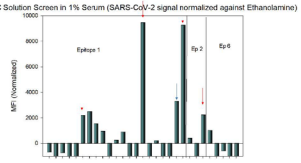

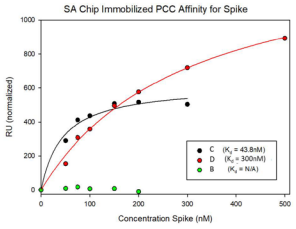

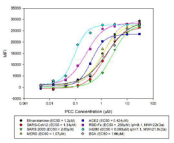

Solution K_d Values of PCC Leads for Various Protein Targets (μM)								
PCC	Ethanolamine	SARS-CoV-2	SARS 2003	MERS	ACE2	RBD-Fc	Int280	BSA
A	28	16.1	13.5	18.7	14	28	7.6	29.7
B	15.8	-	20	55	5.1	6.7	734	-
C	-	17	-	6.8	14.4	1.3	0.98	-
D	1.16	0.531	0.931	0.644	0.314	0.496	0.049	2.7
E	1.2	1.34	0.83	1.07	0.419	0.356	0.045	1.06

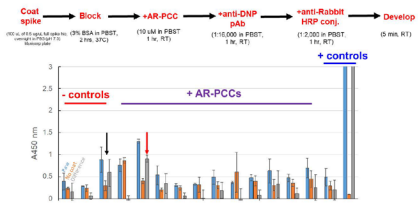

On-going Work

Identified AR-PCC leads have been transitioned to WRAIR for *in vivo* Pharmacokinetic studies. Separate, preliminary testing has demonstrated the ability for PCCs to effectively detect SARS-CoV-2 Spike Protein in 50% Human Serum from a 10 min incubation. This is promising for the development of rapid screening capabilities and further studies will be conducted.

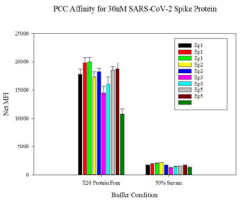

References

- *Wrapp et al. "Cryo-EM structure of the 2019-nCoV spike in the prefusion conformation." Science. 13 March 2020.*
- *https://www.niaid.nih.gov/news-events/novel-coronavirus-sarscov2-images.*
- *Idso, M. et al. Antibody-recruiting protein-catalyzed capture agents to combat antibiotic-resistant bacteria. Chemical Science. 2020, 11, 3054.*
- *Das, S.; Nag, A.; Liang, J. X.; Bunck, D. N.; Umeda, A.; Farrow, B.; Coppock, M. B.; Sarkes, D. A.; Finch, A. S.; Agnew, H. D.; Pitram, S.; Lai, B.; Yu, M. B.; Museth, A. K.; Deyle, K. M.; Lepe, B.; Rodriguez-Rivera, F. P.; McCarthy, A.; Alvarez-Villalonga, B.; Chen, A.; Heath, J.; Stratis-Cullum, D. N.; Heath, J. R., A General Synthetic Approach for Designing Epitope Targeted Macrocyclic Peptide Ligands. Angewandte Chemie-International Edition 2015, 54 (45), 13219-13224.*
- *Coppock, M. B.; Stratis-Cullum, D. N., A universal method for the functionalization of dyed magnetic microspheres with peptides. Methods 2019, 158, 12-16.*

PROCESS MODEL FOR VIRTUAL HEMET MANUFACTURING

POC: Michael Yeager
michael.yeager11.civ@mail.mil

Objective and Challenges

- Current state of the art employs a trial and error approach to thermoplastic composite helmet design
  - Processing science can inform helmet manufacturers of optimal designs and process parameters, eliminating the large time/material cost associated with the trial and error method
  - Goal: To develop a framework for the virtual manufacturing of helmets comprised of extruded UHMWPE laminates, allowing for the optimization of process parameters and stacking sequences

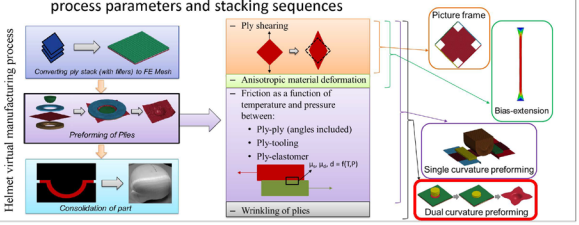

Shear to Thickness Conversion

- Shear and thickness measured on grid
  - –Shear angle measured at each grid points with a Microscribe, image analysis and a goniometer
- Conservation of volume: $t_{deformed} = \frac{t_{undeformed}}{\sin\left(\frac{\pi}{2} - \gamma_{12}\right)}$

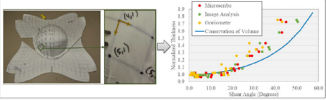

Sheet homogenization

- Homogenization methodology is needed for simulating 50+ sheets
  - Successfully demonstrated for representing up to 10 sheets with a single shell layer

Solutions match for:
- Shear angle
- Punch force

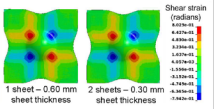

Thermoforming Model Validation

- **Hemisphere:** Model thickness predictions were compared to experimental (CCDC-SC) values (quarter symmetry shown)
  - Below: Percent difference between numerical and experimental results over a range of part thicknesses

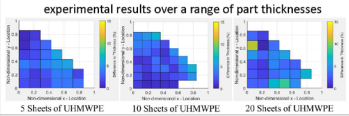

ECH: Model was also validated for the ECH geometry

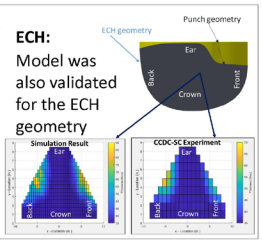

UHMPWE Shear Characterization and Modeling

Picture frame test: Evaluate the ability to predict in-plane shear deformation of UHMPWE fiber system (HB80)

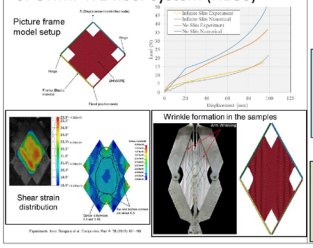

Bias-extension test: Coupling of shear and tension in fiber based (HB210) and film based (Tensylon 30A) UHMWPE systems

- Novel method to calculate τ_{xy}

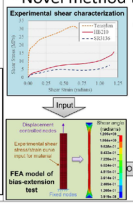

$$\tau_{xy} = \frac{F_y \sin\left(\frac{\pi}{2} - \gamma_{xy}\right)}{2\sqrt{2}\, w\, t_0 \cos\left(\frac{\pi}{4} - \frac{\gamma_{xy}}{2}\right)}$$

- –Geometry: Width (w) and initial thickness (t_0)
- –Instron: Pull force (F_y)
- –DIC: Shear angle (γ_{xy})

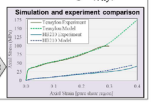

Influence of Shear Response on Final Part

Shear stress vs. strain curves explored:

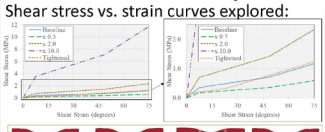

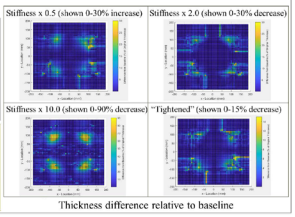

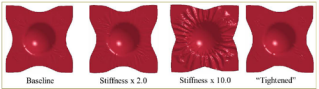

List of Symbols, Abbreviations, and Acronyms

5PECRD	5th Annual Postdoc and Early Career Research Day
ALC	Adelphi Laboratory Center
APG	Aberdeen Proving Ground
ARL	Army Research Laboratory
CCDC	US Army Combat Capabilities Development Command (obsolete acronym)
CISD	Computational and Information Sciences Directorate
HRED	Human Research and Engineering Directorate
NPAW	National Postdoc Appreciation Week
PDA	Postdoc Association
Q&A	question and answer
SEDD	Sensors and Electron Devices Directorate
VTD	Vehicle Technology Directorate
WMRD	Weapons and Materials Research Directorate

1 (PDF)	DEFENSE TECHNICAL INFORMATION CTR DTIC OCA
1 (PDF)	DEVCOM ARL FCDD RLD DCI TECH LIB
2 (PDF)	DEVCOM ARL FCDD RLS RP A WILSON FCDD RLC IB P SHARMA